Prediction of flyrock distance in surface mining using a novel hybrid model of Harris Hawks Optimization with multi-strategies-based support vector regression (MSHHO-SVR)

Chuanqi Li[1], Jian Zhou[2*], Kun Du[3*], Danial Jahed Armaghani[4], Shuai Huang[5]

[1] Laboratory 3SR, CNRS UMR 5521, Grenoble Alpes University, Grenoble 38000, France; Email: Chuanqi.Li@univ-grenoble-alpes.fr

[2*] School of Resources and Safety Engineering, Central South University, Changsha 410083, China. Email: j.zhou@csu.edu.cn (**Corresponding Author**)

[3*] School of Resources and Safety Engineering, Central South University, Changsha 410083, China. Email: dukuncsu@csu.edu.cn (**Corresponding Author**)

[4] School of Civil and Environmental Engineering, University of Technology Sydney, Ultimo, NSW 2007, Australia. Email: danial.jahedarmaghani@uts.edu.au

[5] School of Resources and Safety Engineering, Central South University, Changsha 410083, China. Email: 205511038@csu.edu.cn.

Abstract:

To effectively weaken and control the harm of flyrock in open-pit mines, this study aims to develop a novel Harris Hawks optimization with multi-strategies-based support vector regression (MSHHO-SVR) model for predicting the flyrock distance (FD). Several parameters such as hole diameter (H), hole depth (HD), burden to spacing ratio (BTS), stemming (ST), maximum charge per delay (MC), and powder factor (PF) were recorded from 262 blasting operations to establish the FD database. The MSHHO-SVR model was compared the predictive performance with several other models, including Harris Hawks optimization-based support vector regression (HHO-SVR), back-propagation neural network (BPNN), extreme learning machine (ELM), kernel extreme learning machine (KELM), and empirical methods. The root mean square error (RMSE), the mean absolute error (MAE), the determination coefficient (R^2), and the variance accounted for (VAF) were employed to evaluate the model performance. The results indicated that the MSHHO-SVR model not only performed better in the training phase but also obtained the most satisfactory performance indices in the testing phase, with RMSE values of 12.2822 and 9.6685, R^2 values of 0.9662 and 0.9691, MAE values of 8.5034 and 7.4618, and VAF values of 96.6161% and 96.9178%, respectively. Furthermore, the calculation results of the SHAP values revealed that the H is the most critical parameter for predicting the FD. Based on these findings, the MSHHO-SVR model can be considered as a novel hybrid model that effectively addresses flyrock-like problems caused by blasting.

Keywords:

Flyrock distance; Multi-strategies; Harris Hawks optimization; Support vector regression; SHAP values.

- We are committed to improving the prediction performance of the FD in open-pit mines.
- The optimization ability of HHO algorithm is significantly improved by the multi-strategies method
- The proposed MSHHO-SVR model has higher accuracy than published articles in predicting the FD.

1. Introduction

Blasting has been a widely used rock-breaking technique in various fields, particularly in open pit and underground mining (Monjezi et al. 2013; Wang et al. 2018a, 2018b; Li et al. 2022a; Hosseini et al. 2023). However, studies revealed that a significant portion of the energy (over 70%) produced by blasting is wasted, while the remaining energy is utilized to break and displace hard rocks (Khandelwal and Singh 2005; Singh and Singh 2005; Hosseini et al. 2022a, 2022b). Moreover, blasting also raised environmental concerns, particularly in surface mining, as depicted in Fig. 1. Among the various environmental issues, flyrock stands out as the most hazardous and destructive (Faradonbeh et al. 2016; Bakhtavar et al. 2017; Hasanipanah et al. 2017; Mahdiyar et al. 2017; Koopialipoor et al. 2019; Nguyen et al. 2019; Murlidhar et al. 2021). Bajpayee et al. (2004) reported that flyrock was the direct cause of at least 40% of fatal accidents and 20% of serious accidents in blasting accidents. Accordingly, it is extremely meaningful to calculate the flyrock distance (FD) to prevent deaths, damage to equipment, and other serious accidents.

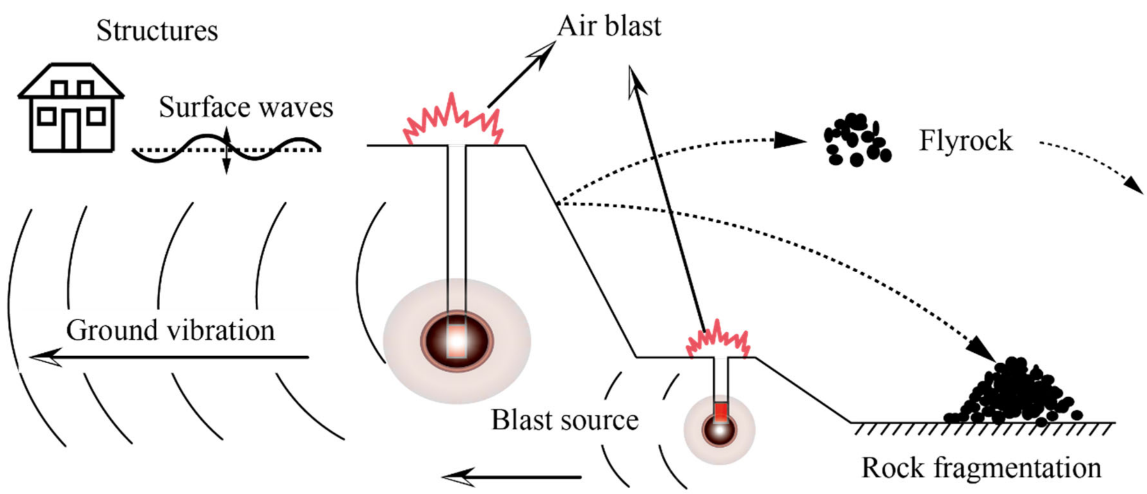

Fig. 1 Negative impacts of blasting in open-pit mines

Reviewing the previous studies (Lundborg et al. 1975; Roth 1979; Gupta 1980; Olofsson 1990; Richards and Moore 2004; McKenzie 2009), a variety of empirical formulas were proposed to predict and control the FD. Bagchi and Gupta (1990) established an empirical formula between stemming (ST), burden (B) and FD. Little (2007) developed an empirical formula based on the drill hole angle, B, ST and explosive charge per meter (CPM) to predict the FD. Trivedi et al.

(2014) also used the ratio of ST to B to establish an empirical equation for estimating the FD. Nevertheless, the prediction performance of the empirical formula is not ideal. The most obvious reason is the absence of valid parameters and the simple consideration of the linear and nonlinear relationship between the parameters and the predicted target (Zhou et al. 2020a, 2020c). In addition to empirical formulas, various researchers have attempted to estimate the FD using statistical analyses, such as Monte Carlo simulation methods, and simple and multiple regression equations (Rezaei et al. 2011; Ghasemi et al. 2012; Raina et al. 2014; Armaghani et al. 2016; Faradonbeh et al. 2016; Ye et al. 2021). However, the regression and simulation models have obvious shortcomings, respectively: a) newly data other than the original data can reduce the reliability of the regression model (Marto et al. 2014); b) historical database cannot be used to control/determine input distribution of the simulation model (Little and Blair 2010). Generally, there are two types of parameters that contribute to estimating the FD: controllable and uncontrollable. The controllable parameters, commonly referred to as blast design parameters, including hole diameter (H), B, ST, CPM, powder factor (PF), spacing (S), total charge, hole depth (HD), and delay timing (Rezaei et al. 2011; Trivedi et al. 2015; Rad et al. 2018; Han et al. 2020; Zhou et al. 2020a). These parameters can be manually adjusted and have a direct impact on the generation of flyrock. Fig. 2 illustrates several potential conditions and the corresponding mechanisms that induce face bursting. Furthermore, if the ratio of ST to H is small and the stemming quality is poor, it may lead to cratering and rifling (Lundborg and Persson 1975; Ghasemi et al. 2012; Saghatforoush et al. 2016; Hasanipanah et al. 2018a). In contrast, uncontrollable parameters refer to characteristic indices related to the physical properties of the rock mass, such as rock density (RD), blastability index (BI), and block size (BS) (Monjezi et al. 2010, 2012; Hudaverdi and Akyildiz 2019), geological properties of the rock mass including the geological strength index (GSI), the rock mass rating (RMR), the rock quality designation (RQD), and the uniaxial compressive strength (UCS) (Trivedi et al. 2015; Asl et al. 2018), as well as environmental factors like the weathering index (WI) (Murlidhar et al. 2021).

Over the past few years, a broad spectrum of artificial intelligence (AI) algorithms represented by machine learning (ML) models has been developed and employed to forecast the FD based on both controllable and uncontrollable parameters, as summarized in Table 1. In general, a single ML method was usually employed to predict the FD, e.g., artificial neural network (ANN) (Monjezi et al., 2010, 2011; Hosseini et al. 2022; Wang et al. 2023), least squares-support vector machine (LS-

SVM) (Rad et al. 2018), extreme learning machine (ELM) (Lu et al. 2020), support vector regression (SVR) (Armaghani et al. 2020; Guo et al. 2021b), back-propagation neural network (BPNN) (Yari et al. 2016), adaptive neuro-fuzzy inference system (ANFIS) (Armaghani et al. 2016), random forest (RF) (Han et al. 2020; Ye et al. 2021), and deep neural network (DNN) (Guo et al. 2021a). Nonetheless, most single ML models, particularly ANN, SVR, RF, and ANFIS, who have low learning rates and are easy to fall into local optimum (Wang et al. 2004; Moayedi and Armaghani 2018; Li et al. 2022a, 2022b). However, it is extremely time-consuming and difficult to select hyperparameter parameters of a single ML model by manual methods for solving complex problems (Li et al. 2022d). In other words, the hyperparameter selection problem can also be considered as an optimization problem. Recently, the use of metaheuristic algorithms is an effective method for solving optimization problems (Monjezi et al. 2012; Armaghani et al. 2014; Kumar et al. 2018). Besides, the metaheuristic algorithms have been noticed and used to improve the predictive ability of traditional ML models in solving engineering problems, including evolution-based (Majdi and Beiki 2010; Yagiz et al. 2018; Zhang et al. 2022), physics-based (Khatibinia and Khosravi 2014; Liu et al. 2020; Momeni et al. 2021), and swarm-based methods (Zhou et al. 2019, 2020a, 2020b, 2021b, 2021c; Li et al. 2022a, 2022b; Adnan et al. 2023a, 2023b; Ikram et al. 2023a). Swarm-based optimization methods, such as the Grey wolf optimization algorithm (GWO), Sparrow search algorithm (SSA), and Harris Hawks optimization (HHO), offer the advantage of requiring only a few parameters, namely population and iteration, to be adjusted in order to enhance the optimized performance (Kardani et al. 2021; Li et al. 2021d; Zhou et al. 2021a). To improve the accuracy of single ML model for predicting the FD, researchers have applied various metaheuristic algorithms-based swarm to the hyperparameter optimization of ML models (Hasanipanah et al. 2016, 2018b; Murlidhar et al. 2020, 2021; Guo et al. 2021b; Kalaivaani et al. 2020; Nguyen et al. 2021; Fattahi and Hasanipanah 2022). However, the performance of metaheuristic algorithms-based swarm is limited by the lack of initial population diversity (Zhou et al. 2022). Meanwhile, the low precision convergence and convergence time of such metaheuristic algorithms in the optimization of multi-dimensional complex problems have already become traditional weaknesses (Li et al. 2021c).

Therefore, the objective of this study is to develop a novel and comprehensive optimization model, which combines multi-strategies (MS) and HHO algorithm to optimize SVR model for predicting the FD. The proposed model is named the MSHHO-SVR model. A database was created based on the monitoring of 262 blasting operations from various open-pit mines, where a series of influence parameters related to the FD were collected. Three other ML models and an empirical equation were also developed to predict the FD and were compared with the HHO-SVR model and MSHHO-SVR model. The prediction performance of all models was evaluated using root mean square error (RMSE), mean absolute error (MAE), determination coefficient (R^2), and variance accounted for (VAF) in both training and testing phases. Additionally, the Shapley additive explanations (SHAP) method, an emerging additive explanatory method, was employed to calculate the influence of the input parameters on FD in the sensitivity analysis.

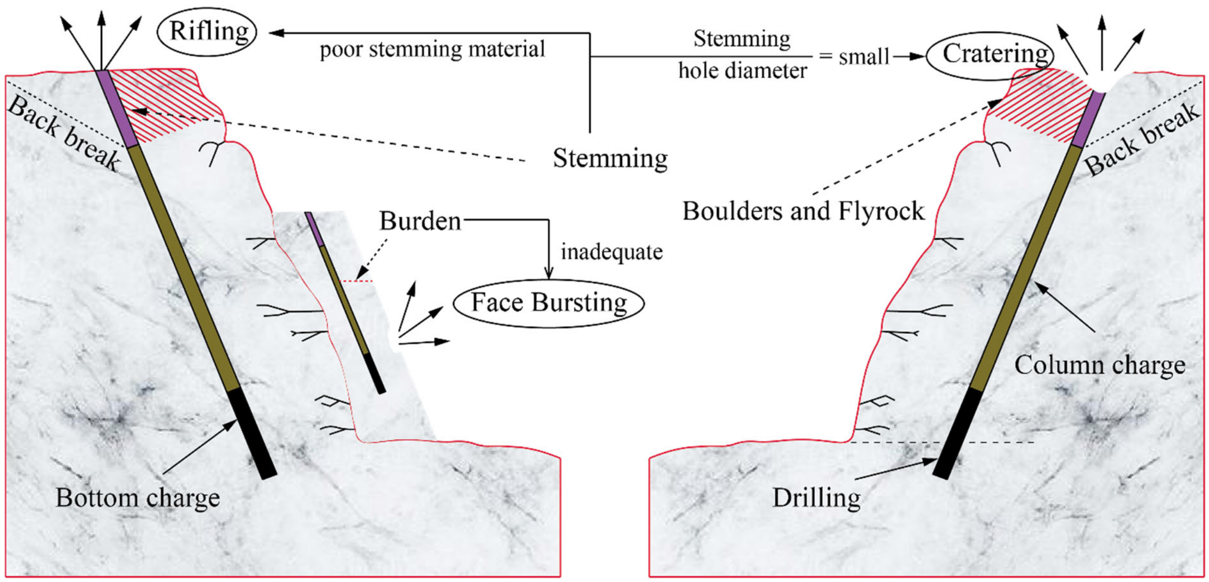

Fig. 2 Three important Flyrock generation mechanisms

Table 1 Reviewed ML models for predicting the FD

ML models	Parameter		No. data	Reference
	Controllable	Uncontrollable		
ANN	PF, HD, BTS, MC, SD, N, ST	RD	250	Monjezi et al. (2010)
ANN	PF, H, B, ST, BTS, MC, SD, HD	BI	192	Monjezi et al. (2011)
ANN	H, HD, B, S, Q, CPM	UCS, RQD	125	Trivedi et al. (2015)

ANFIS				
ANN DNN	PF, S, B, H, ST, MC,	-	240	Guo et al. (2021a)
BPNN	PF, B, S, CPM	UCS, RQD	120	Trivedi et al. (2016)
SVR LS-SVM	BH/B, BTS, SD, PF, MC	RD	90	Rad et al. (2018)
ELM	S, B, PF, ST	RD	82	Lu et al. (2020)
RF	PF, H, BS, MC, HD, ST	-	262	Ye et al. (2021)
GA-ANN	PF, B, S, SD, MC, HD, ST	RMR	195	Monjezi et al. (2012)
PSO-ANN	B, S, MC, SD, H, ST, N, PF	RD	44	Armaghani et al. (2014)
PSO-RFNN	B, MC, S, ST	-	72	Kalaivaani et al. (2020)
PSO-ANN	HD, ST, PF, MC, B, S	-	65	Zhou et al. (2020c)
FA-ANN	BTS, ST, HD, MC, PF	RD, Rn	113	Li et al. (2021f)
WOA-DNN	PF, MC, S, B, ST, HD	-	240	Guo et al. (2021a)
HHO-MLP	PF, H, ST/B, HD, CPM	GSI, RQD, WI	152	Murlidhar et al. (2021)
WOA-SVM	PF, B, W, S, ST	-	210	Nguyen et al. (2021)
GOA-ANFIS	PF, S, B, ST	RD	80	Fattahi and Hasanipanah (2022)

Note: No. data: the number of considered samples in dataset; BTS= Burden to Spacing ratio; MC= Maximum charge per delay (kg); SD= Specific drilling (m/m^3); BH= Bench height (m); Q= Charge per blast hole (kg); N= Number of rows; Rn= Schmidt hammer rebound number; ST/B= Stemming to burden ratio; W= Per blast; GOA-Grasshopper optimization algorithm; GA-Genetic algorithm; FA-Firefly algorithm; RFNN-recurrent fuzzy neural network; WOA-Whale optimization algorithm; HHO-Harris Hawks optimization; PSO-Particle swarm optimization.

2. Methodologies

2.1 Support vector regression

SVR is a specialized algorithm within the support vector machines (SVM) family that was developed by Vapnik (1995) for resolving regression problems. For the SVR algorithm, the structural risk minimization (SRM) is the core of the optimizer algorithm used to obtain the minimum training error (Li et al. 2021b). In other words, the nonlinear regression prediction is also a function fitting problem by using SVR model, which can be described as follows:

$$f(z) = w\Psi(z) + b \tag{1}$$

where w represents a weight vector. $\Psi(z)$ describes a nonlinear mapping between input space and high-dimensional space. b represents a model error also called threshold value. Then, the minimization of w and b can be calculated according to the SRM as in Eq. (2).

$$\begin{gathered}\text{Minimize}: C(\nu\vartheta + \frac{1}{M}\sum\nolimits_{i=1}^{M}(\zeta_i, \zeta_i^*)) + \|W\|^2/2 \\ \text{Subject to} \begin{cases} (w\Psi(z_i)+b_i) - s_i \leq \vartheta + \zeta_i, i = 1,2,\ldots,M \\ s_i - (w\Psi(z_i)+b_i) \leq \vartheta + \zeta, i = 1,2,\ldots,M \\ \zeta_i^* \geq 0, \vartheta \geq 0, i = 1,2,\ldots,M \end{cases}\end{gathered} \tag{2}$$

Finally, the Eq. (1) is rewritten as follows:

$$f(z) = \sum\nolimits_{j=1}^{M}\left(\delta_i - \delta_i^*\right)\kappa\left(z_i, z_j\right) + b \tag{3}$$

where C represents penalty factor for balancing the model smoothness. ζ_i and ζ_i^* represent the slack parameters. M denotes the number of pattern records. $\|W\|^2/2$ represents the smoothness, and the ϑ is set to the default value of 0.1. $\kappa\left(z_i, z_j\right) = \Psi(z_i)\Psi(z_j)$ indicates the kernel function. In this study, the radial basis function (RBF) is employed as a widely used kernel function to solve the prediction problem. Therefore, C and the kernel parameter (γ) are the main hyperparameters of SVR model in this study.

2.2 Harris Hawks optimization

The HHO algorithm, developed by Heidari et al. (2019), is an emerging metaheuristic optimization algorithm, which is inspired by the unique cooperative hunting activities of Harris's hawk in nature called "surprise pounce". For solving the optimization problems, each Harris's hawk can be considered as a candidate solution, and the best solution is faulty when considered as the prey. As shown in Fig. 3a, the standard HHO is split into two parts named the exploration and the exploitation, as well as different perching and attacking strategies.

Exploration is the beginning of a successful foraging campaign. Harris's hawks use their dominant eyes to search for and track prey. Especially when prey is highly alert, they wait, observe, and monitor for about 2 hours. There are two different perching strategies that can be executed with the same probability or chance, which are expressed mathematically as:

$$X(n+1)=\begin{cases} X_{rand}(n)-r_1\left|X_{rand}(n)-2r_2X(n)\right| & q\geq 0.5 \\ (X_{prey}(n)-X_m(n))-r_3(L_B+r_4(U_B-L_B)) & q<0.5 \end{cases} \tag{4}$$

where $X(n)$ and $X(n+1)$ denote the positions of hawks in the n-th iteration and the $n+1$-th iteration, respectively. $X_{rand}(n)$ and $X_{prey}(n)$ illustrate the positions of the randomly selected hawk and prey in n-*th* iteration, respectively. The parameters q, r_1, r_2, r_3, and r_4 represent random numbers varying from 0 to 1 in each iteration. L_B and U_B delegate the lower and upper boundaries of the internal parameters, respectively. Notably, the mean position of the hawks ($X_m(n)$) is expressed in Eq. (5).

$$X_m(n)=\frac{1}{I}\sum_{i=1}^{I}X_i(n) \tag{5}$$

where I is the number of Harris's hawks, and $X_i(n)$ illustrates the position of the i-*th* individual hawk in the n-th iteration.

After identifying the prey and its location, the hawks can select from a range of attacking strategies based on the available energy. The energy consumption during the attack is mathematically expressed as follows:

$$E=2E_0(1-\frac{n}{T}) \tag{6}$$

where E and E_0 represent the escaping energy and initial energy of the prey, respectively. n indicates the current iteration, and the maximum number of iterations is illustrated by T in the HHO algorithm. When E is less than 1, hawks continue to stay in exploration phase to obtain a better prey. On the contrary, hawks start to execute different attack strategies to hunt prey in exploitation phase.

In exploitation phase, hawks can choose the appropriate attacking strategy according to the different escape behaviors and energy surplus of prey. Assuming the prey has an escape chance of prey is E_c, then the chances of successful escape and capture are expressed as $E_c \geq 0.5$ or $E_c < 0.5$. Combining the escaping energy of prey, there are four possible attacking strategies selected by hawks to hunt prey, as written in Eqs. (7)- (10).

No. 1. Soft besiege: This attack strategy is triggered once the prey (e.g., rabbit) has enough escape energy ($|E| \geq 0.5$) but still did not escape out of hawk's territory ($E_c \geq 0.5$).

$$\begin{aligned} X(n+1) &= \Delta X(n) - E\left|JX_{prey}(n) - X(n)\right| \\ \Delta X(n) &= X_{prey}(n) - X(n) \end{aligned} \tag{7}$$

No. 2. Hard besiege: Once the escape energy of prey is exhausted ($|E| < 0.5$) but it still does not escape the hawk's territory ($E_c \geq 0.5$), hawks initiate the hard besiege strategy to capture the prey.

$$X(n+1) = X_{prey}(n) - E\left|\Delta X(n)\right| \tag{8}$$

No. 3. Soft besiege with progressive rapid dives (see Fig. 3b): When the prey has enough escape energy ($|E| \geq 0.5$) and can use different deceptive behaviors to escape the hawk's territory ($E_c < 0.5$).

$$\begin{aligned} Y &= X_{prey}(n) - E\left|JX_{prey}(t) - X(n)\right| \\ Z &= Y + S \times LF(D) \\ X(n+1) &= \begin{cases} Y & \text{if } Fitness(Y) < Fitness(X(n)) \\ Z & \text{if } Fitness(Z) < Fitness(X(n)) \end{cases} \end{aligned} \tag{9}$$

No. 4. Hard besiege with progressive rapid dives (see Fig. 3c): If the prey has less escape energy ($|E| < 0.5$) while can take different deceptive behaviors to escape the hawk's territory ($E_c < 0.5$), hawks try to save more moving distance for hunting the prey. This trigger condition of No. 4 strategy is similar to No. 3.

$$\begin{aligned} Y^* &= X_{prey}(n) - E\left|JX_{prey}(t) - X_m(n)\right| \\ Z^* &= Y^* + S \times LF(D) \\ X(n+1) &= \begin{cases} Y^* & \text{if } Fitness(Y^*) < Fitness(X(n)) \\ Z^* & \text{if } Fitness(Z^*) < Fitness(X(n)) \end{cases} \end{aligned} \tag{10}$$

where $\Delta X(n)$ represents the difference of position between prey and hawk in the *n-th* iteration. J represents the intensity of escape movement, which is changed randomly between 0 and 2. D and

S express the dimension of searching space and a random vector, respectively. *Fitness* () represents the fitness evaluation function in iteration. *LF* describes the levy flight function, which can be written as:

$$LF(x) = 0.01 \times \frac{\mu \times \sigma}{|\upsilon|^{\frac{1}{\beta}}}, \sigma = \left(\frac{\Gamma(1+\beta) \times \sin\left(\frac{\pi\beta}{2}\right)}{\Gamma(\frac{1+\beta}{2}) \times \beta \times 2^{(\frac{\beta-1}{2})}} \right)^{\frac{1}{\beta}} \tag{11}$$

where μ and υ represent random values changed in the range of [0, 1]. β represents a constant, which is set to 0.5 by default in the HHO algorithm.

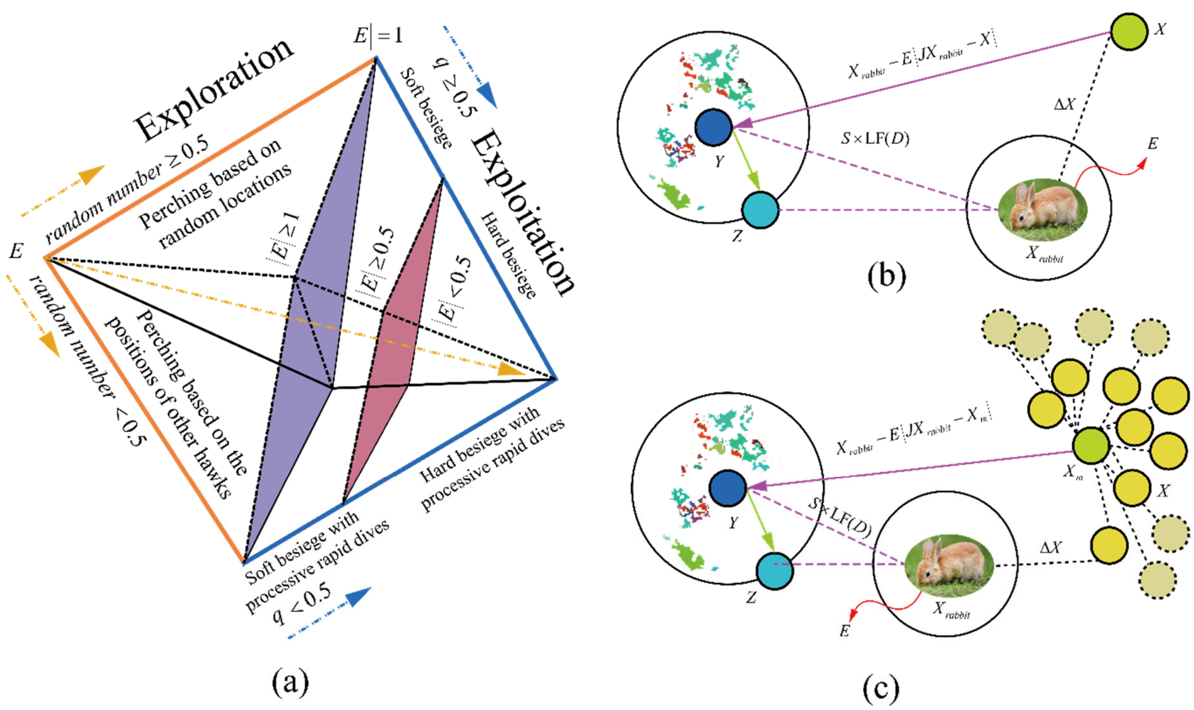

Fig. 3 A standard HHO algorithm: (a) All phases; (b) Soft besiege with progressive rapid dives; (c) Hard besiege with progressive rapid dives

2.3 Harris Hawks optimization with Multi-strategies (MSHHO)

Despite the extensive use of the HHO algorithm in solving various engineering problems by many researchers (Moayedi et al. 2020; Murlidhar et al. 2021; Zhang et al. 2021; Zhou et al. 2021d; Kaveh et al. 2022), it still faces the challenge of low convergence accuracy and premature convergence while dealing with high-dimensional and complex optimization problems. To address these issues, several methods have been proposed to enhance the performance of the HHO algorithm, including chaotic local search (Elgamal et al. 2020), self-adaptive technique (Wang et al. 2021; Zou and Wang 2022), hybridizing supplementary algorithms (Fan et al. 2020; Hussain et al. 2021). In any case, the goal of improving HHO is to optimize the initial HHO algorithm's exploration and exploitation. In this study, three strategies named chaotic mapping, Cauchy mutation, and adaptive weight are used to enhance the performance of the initial HHO algorithm.

(1) Chaotic mapping

Several studies have shown that chaotic mapping can be used to create a more diverse population by using chaotic sequences (Kohli and Arora 2018). Among chaotic mapping functions, logistic mapping is widely used to rich the diversity of population for improving the performance of metaheuristic algorithms (Hussien and Amin 2022). Therefore, the initial population of the HHO was generated by using a logistic mapping as written as Eq. (12). Then, the novel candidate solution generated can be obtained as:

$$Log^{s+1} = \kappa Log^{s}(1 - Log^{s}) \quad 0 \le \kappa \le 4 \tag{12}$$

$$Cs = TP \times (1 - \varepsilon) + \varepsilon C'_i, \quad i = 1, 2, \ldots, s \tag{13}$$

where Log^{s+1} and Log^{s} represent the s+1 and s order chaotic sequence, respectively. κ represents a constant between 0 and 4. C_s delegates the candidate solution. TP illustrates the target position. C' represents the maps. And ε represents a factor related to the iteration, which is calculated as follows:

$$\varepsilon = \frac{Max_{iteration} - Cur_{iteration} + 1}{Max_{iteration}} \tag{14}$$

where $Max_{iteration}$ represents the maximum number of iterations, and $Cur_{iteration}$ indicates the current iteration.

(2) Cauchy mutation

The Cauchy distribution function is a simple yet effective method to address the problem of metaheuristic algorithms being susceptible to local optima (Yang et al., 2018). The Cauchy variation can augment the diversity of the population in the search space of hawks, thereby improving the global search capability of the original HHO algorithm. The mathematical representation of Cauchy mutation is written as:

$$f(x) = \frac{1}{\pi}\left(\frac{1}{x^2+1}\right) \tag{15}$$

After applying the Cauchy mutation, the search algorithm can explore more global optima:

$$X_{best}^{*} = X_{best} + X_{best} \times Cauchy(0,1) \tag{16}$$

(3) Adaptive weight

In this study, an adaptive weight method was employed to update the position of prey during the exploitation phase in the HHO algorithm. The adaptive weight factor (w_f) has different functions in improving the performance of local optimization, such as a smaller w_f can increase the exploitation time and result in a better solution. This process is represented by Eq. (17) and Eq. (18).

$$w_f = \sin\left(\frac{\pi \times Cur_{iteration}}{2Max_{iteration}} + \pi\right) + 1 \tag{17}$$

$$X_{prey}^{*}(t) = w_f \times X_{prey}(t) \tag{18}$$

The framework of using Harris Hawks optimization with Multi-strategies (MSHHO)- based SVR model to predict the FD is shown in Fig. 4. Besides, four comparison models were established to compare the predictive performance with the HHO and MSHHO- based SVR models, including ELM, KELM, BPNN, and empirical models. The principles of these models above were described in detail as follows literature (Roth 1979; Huang et al. 2006; McKenzie 2009; Chen et al. 2016; Yari et al. 2016; Zhang and Goh 2016; Wang et al. 2017; Elkatatny et al. 2018; Luo et al. 2019; Shariati et al. 2020; Jamei et al. 2021). To accurately learn relationship between the input parameters and the FD, the database was divided into two subsets, i.e., training set and test set (30% of the total data). Noted that all data should be normalized into the range of 0 to 1 or -1 to 1. The latter is considered in this study. Furthermore, the fitness function built by Root mean square error (RMSE) is set as the only criterion for evaluating the performance of each hybrid model. The better model with the suitable hyperparameters has lower value of fitness than other models. Finally, all developed models should be evaluated using performance indices or other evaluation approaches (e.g., regression analysis, Taylor diagrams).

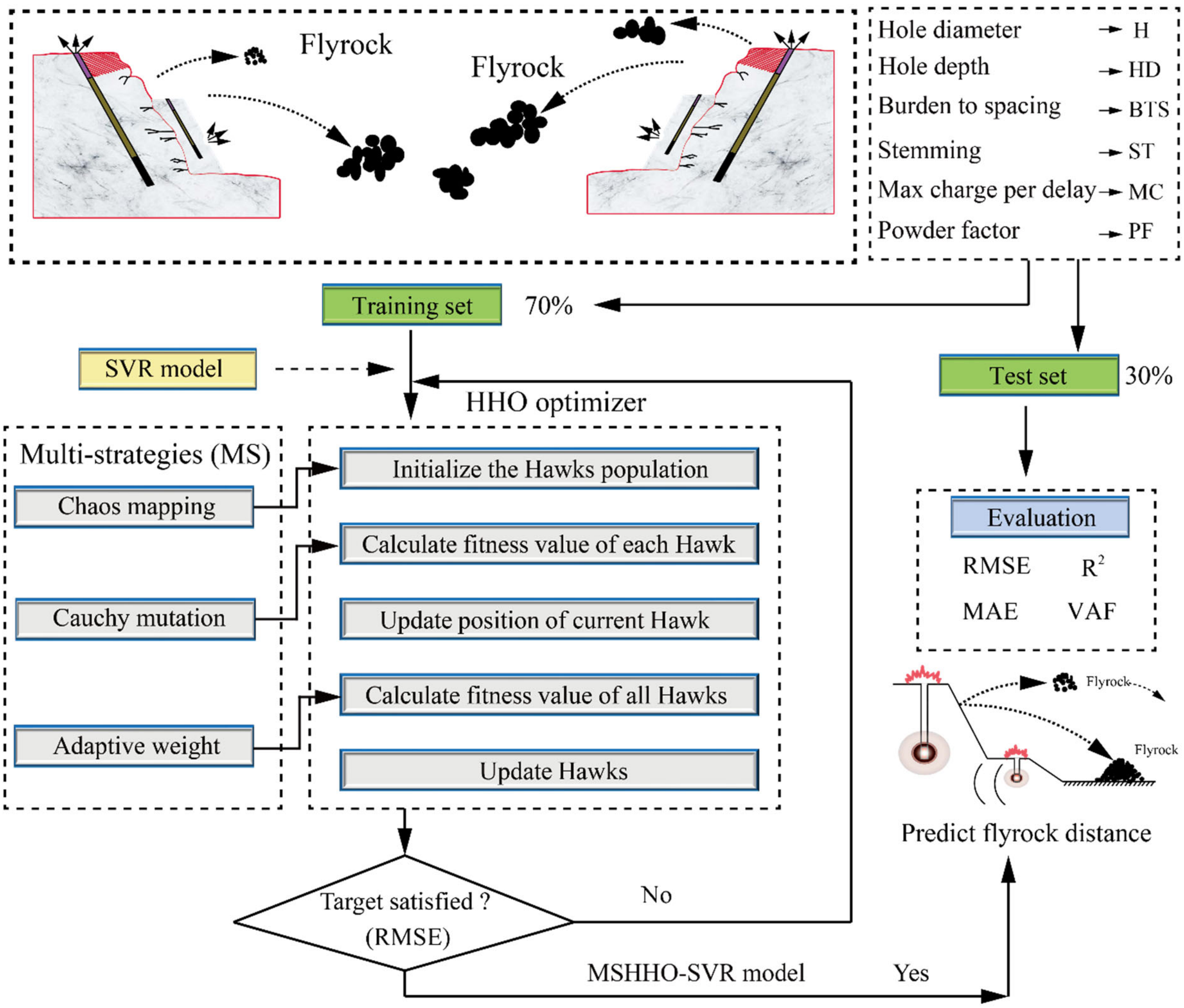

Fig. 4 The framework of FD prediction

3. Study site and Dataset

In order to forecast the flyrock phenomenon, six open pit mines (i.e., Taman Bestari, Putri Wangsa, Trans Crete, Ulu Tiram, Masai, and Ulu Choh) were investigated in Malaysia. Their locations are shown in Fig. 5. A big data survey showed that the total amount of blasting in these mines reached 240,000 tonnes a year, with an average of 15 large-scale blasting operations carried out every month (Han et al. 2020). The blasting operation with high charge and high frequency is bound to cause a serious flyrock phenomenon (see Fig. 5). According to Table 1, different controllable and uncontrollable parameters were used as predictors in previous flyrock studies. In this study, we monitored 262 blasts and recorded six individual influence parameters, namely H, HD, BTS, ST, MC, and PF, as input parameters to predict the FD. Although uncontrollable parameters of RQD and Rn were also measured, only the range values were recorded and could not be adopted in this study. Fig. 6 shows the distribution of the input parameters.

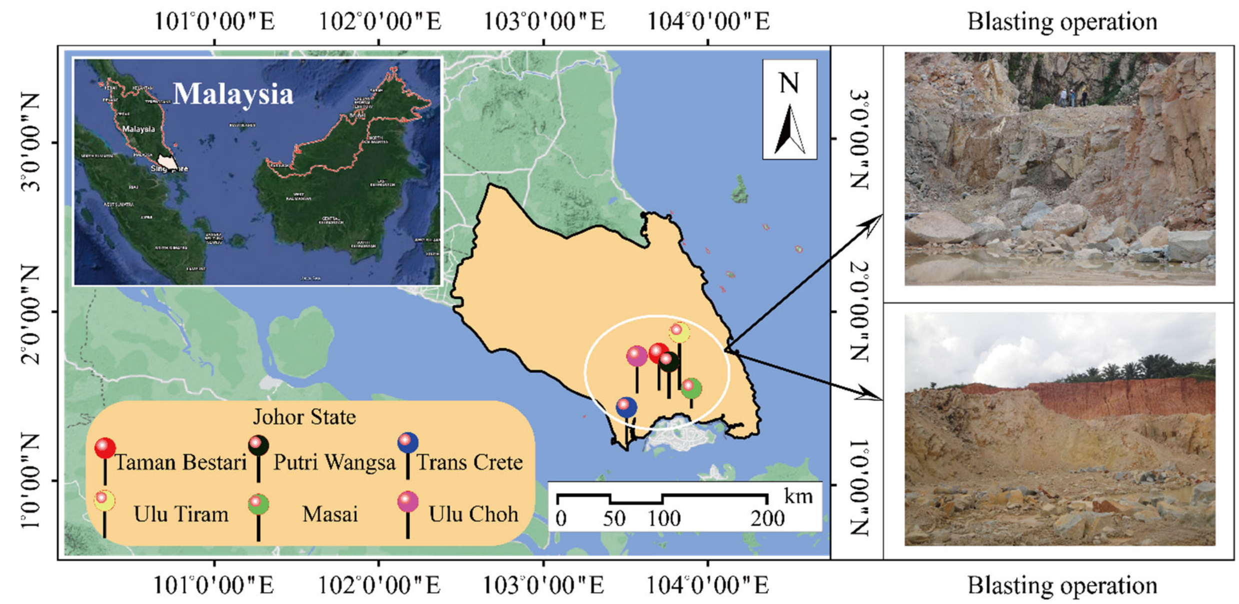

Fig. 5 Locations of six open pit mines in Malaysia used for predicting the FD

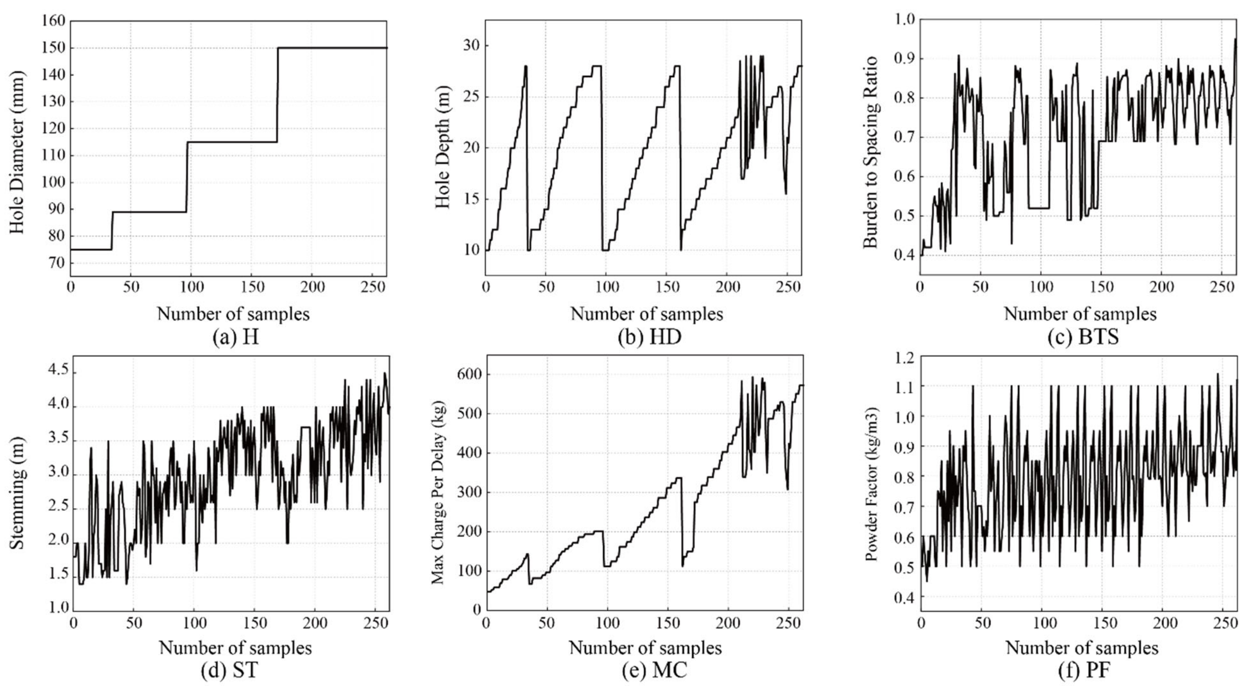

Fig. 6 Distribution pattern of input parameters

Fig. 7 displays the correlation coefficients and data distributions of the input parameters and output parameters. The purpose of correlation analysis is to select the appropriate parameters to build the prediction model. If two parameters that are highly correlated with each other are a burden to build the model because their contributions to the target prediction are approximate. On the other hand, the direct correlation coefficient (R) between an input parameter and the predicted target is large, it indicates that the input parameter has a key influence on whether the target can be accurately predicted. As shown in this picture, the values of R between input parameters are low, and each input parameter has a good linear relationship with the FD. Therefore, the six parameters selected can be used to build the prediction model.

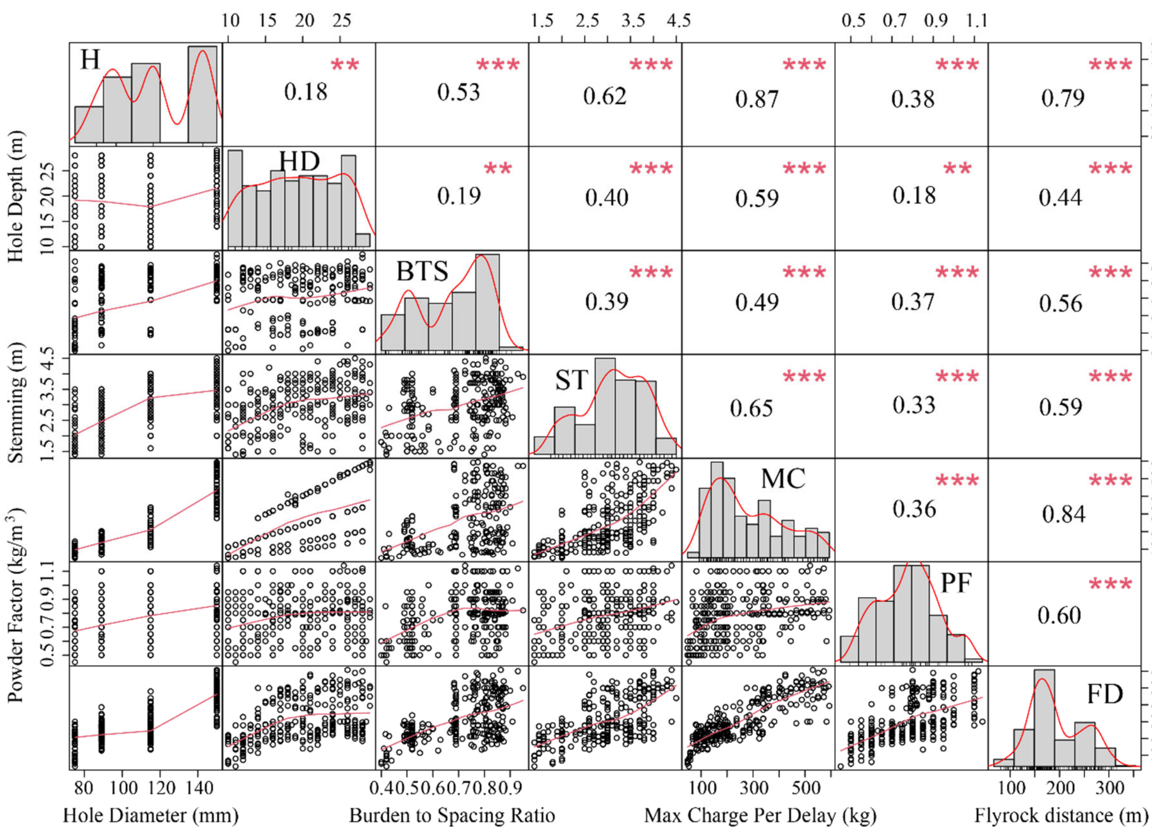

Fig. 7 Correlations between input and output parameters

4. Model evaluation

To evaluate the reliability and accuracy of the proposed model, as well as three other ML models and an empirical formula for predicting the FD, it is necessary to apply statistical indices to quantify their predictive performance. RMSE, R^2, mean absolute error (MAE), and variance accounted for (VAF) are widely utilized as performance indices in model evaluation, as reported in several published studies (Hasanipanah et al. 2015; Armaghani et al. 2021; Li et al. 2022c; Murlidhar et al. 2021; Jamei et al. 2021; Ikram et al. 2022a, 2022b, 2023b; Du et al. 2022; Dai et al. 2022; Mikaeil et al. 2022). These aforementioned indices are defined in equations (19) to (22).

$$\mathrm{RMSE}=\sqrt{\frac{1}{U}\sum_{u=1}^{U}\left(FD_{o,u}-FD_{p,u}\right)^{2}} \tag{19}$$

$$\mathrm{R}^{2}=1-\frac{\left[\sum_{u=1}^{U}(FD_{o,u}-FD_{p,u})\right]^{2}}{\left[\sum_{u=1}^{U}(FD_{o,u}-\overline{FD_{o}})\right]^{2}} \tag{20}$$

$$\mathrm{MAE}=\frac{1}{U}\sum_{u=1}^{U}\left|FD_{o,u}-FD_{p,u}\right| \tag{21}$$

$$\mathrm{VAF}=\left[1-\frac{\mathrm{var}(FD_{o,u}-FD_{p,u})}{\mathrm{var}(FD_{o,u})}\right]\times 100\% \tag{22}$$

where U represents the number of used samples in the training or testing phase. $FD_{o,u}$ and $\overline{FD_{o}}$ indicate observed FD value of the u-th sample and mean of observed FD values, respectively. $FD_{p,u}$ indicates the predicted FD value of the u-th sample.

5. Developing the models for predicting FD

In this study, an enhanced HHO algorithm with multi-strategies was employed to select the hyperparameters of SVR model for predicting the FD. The other five different models, i.e., HHO-SVR, ELM, KELM, BPNN, and empirical formula, have also been considered and compare the predictive performance with the proposed MSHHO-SVR model. The procedures for model development and assessment are described in the following sections.

5.1 Evaluation performance of MSHHO model

As previously mentioned in Section 2.3, the logistic mapping of chaotic sequences is used to initialize the population of HHO for increasing swarm diversity, the Cauchy mutation is utilized to expand the search space and improve the global search capability (i.e., exploration) of HHO, and the local optimization capability (i.e., exploitation) is improved by assigning the adaptive weight strategy. Three MSHHO algorithms are generated by using the aforementioned strategies, namely, HHO-Logistic mapping (HHO-Log), HHO-Cauchy mutation and adaptive weight (MHHO), and MHHO-Log. To compare the performance of MSHHO algorithms with the initial HHO, six benchmark functions consisting of three unimodal functions and three multimodal functions are used to obtain the objective function values as shown in Table 2. The performance of different algorithms can be demonstrated by the average (Aver) and standard deviation (St. D) values of their objective functions. To balance out the interference of other conditions, the dimension and iteration time are set as 30 and 200 in each algorithm. Besides, the initial population is given three values (25, 50 and 75) to increase the complexity and reliability of the verification. The results of performance evaluation for all algorithms are shown in Table 3. As can be seen in this table, all enhanced HHO algorithms obtained better performance than the unchanged HHO algorithm by resulting in lower values of Aver and St. D of objective functions, especially for the MHHO-Log algorithm. It can be noted that each algorithm has the best performance with a population of 50 in different functions. Fig. 8 and Fig. 9 reflect the dynamic convergence performance of all algorithms based on the unimodal and multimodal benchmark functions during 200 iterations, respectively. It is obvious that the MHHO-Log has the lowest values of objective function in F_6 when the population is 50. Furthermore, the performance of all MSHHO algorithms has been improved to be superior to HHO by adjusting the population, the capability of global search and local optimization.

Table 2 Benchmark functions adopted in this study

Type	Function Name	Function description	Initial range
Unimodal	Sphere	$F_1 = \sum_{i=1}^{d} x_i^2$	[-100, 100]
Unimodal	Noise	$F_2 = \sum_{i=1}^{d} i x_i^4 + random\left[0,1\right)$	[-1.28, 1.28]
Unimodal	Rosenbrock	$F_3 = \sum_{i=1}^{d-1} \left[100(x_{i+1} - x_i^2)^2 + (x_i^2 - 1)^2\right]$	[-30, 30]
Multimodal	Schwefel's 2.26	$F_4 = \sum_{i=1}^{d} -x_i \sin\left(\sqrt{\lvert x_i \rvert}\right)$	[-500, 500]
Multimodal	Rastrigin	$F_5 = \sum_{i=1}^{d} \left[x_i^2 - 10\cos\left(2\pi x_i\right) + 10)\right]$	[-5.12, 5.12]
Multimodal	Griewank	$F_6 = \frac{1}{4000} \sum_{i=1}^{d} x_i^2 - \prod_{i=1}^{d} \cos\left(\frac{x_i}{\sqrt{i}}\right) + 1$	[-600, 600]

Table 3 Results of six testing bench functions with different HHO algorithms

Algorithms	Pop	F_1		F_2		F_3	
		Aver	St. D	Aver	St. D	Aver	St. D
HHO	25	958.30	9819.90	3147268.49	37724594.73	1.25	8.95
HHO-Log	25	884.88	9062.11	2664563.15	37682586.34	1.25	8.91
MHHO	25	553.68	7830.15	1660512.01	21134739.95	0.70	6.34
MHHO-Log	25	543.57	5503.58	1082928.33	14059789.16	0.50	6.89
Algorithms	Pop	F_4		F_5		F_6	
		Aver	St. D	Aver	St. D	Aver	St. D
HHO	25	-11868.84	1873.87	10.12	62.45	7.86	77.15
HHO-Log	25	-12035.37	1813.46	6.65	47.89	5.26	68.42
MHHO	25	-12082.34	1801.08	4.63	46.13	4.03	43.36
MHHO-Log	25	-12297.91	1319.68	4.42	36.54	3.35	38.24
Algorithms	Pop	F_1		F_2		F_3	
		Aver	St. D	Aver	St. D	Aver	St. D
HHO	50	685.80	7988.11	2613611.52	34632259.44	0.99	7.70
HHO-Log	50	553.68	7830.15	1983466.58	28050439.55	0.76	7.67
MHHO	50	390.24	4523.87	1444017.08	19812892.09	0.48	6.75
MHHO-Log	50	319.37	4516.29	1074024.53	15186980.00	0.40	5.68
Algorithms	Pop	F_4		F_5		F_6	
		Aver	St. D	Aver	St. D	Aver	St. D
HHO	50	-11942.22	1928.83	9.68	57.17	2.95	41.64
HHO-Log	50	-12315.82	1179.94	4.62	43.61	0.29	2.03
MHHO	50	-12305.10	1184.75	4.49	35.62	0.42	2.34
MHHO-Log	50	-12362.58	1174.31	3.20	33.85	0.11	1.49
Algorithms	Pop	F_1		F_2		F_3	
		Aver	St. D	Aver	St. D	Aver	St. D
HHO	75	740.03	8283.89	2856687.80	35933361.47	1.16	8.42
HHO-Log	75	633.58	7566.86	2289411.71	32377154.01	0.96	8.26
MHHO	75	452.39	4858.62	1898283.72	21744332.20	0.65	5.69

MHHO-Log	75	353.31	4996.37	1244797.51	15878824.11	0.44	6.09
Algorithms	Pop	F_4		F_5		F_6	
		Aver	St. D	Aver	St. D	Aver	St. D
HHO	75	-11910.08	1801.17	14.33	49.16	6.19	70.05
HHO-Log	75	-12046.67	1314.03	8.45	48.63	4.06	47.07
MHHO	75	-11986.09	1650.95	6.70	47.96	4.74	67.08
MHHO-Log	75	-12431.06	1107.52	6.63	38.11	2.87	34.54

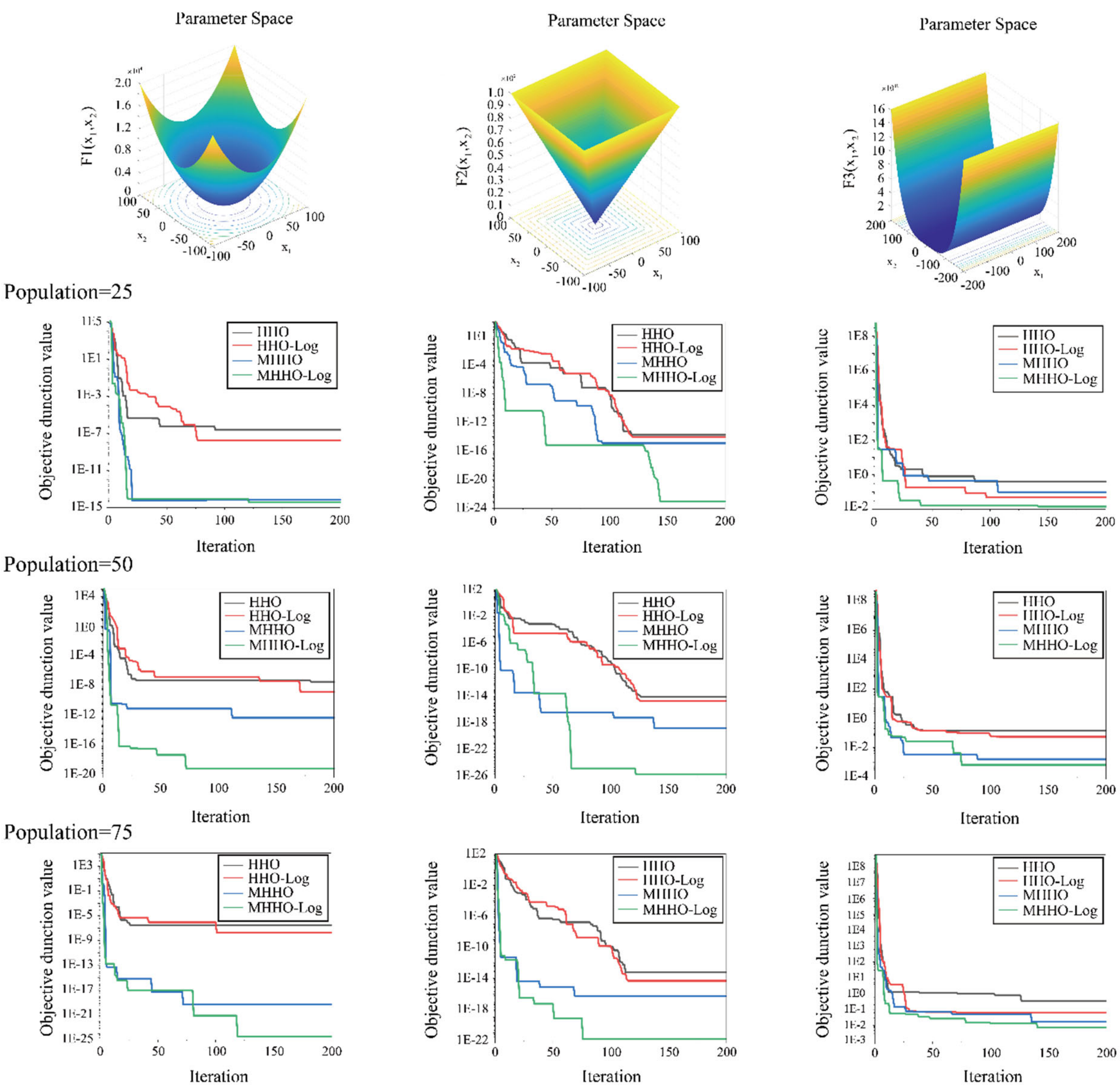

Fig. 8 Comparisons between HHO and MSHHO by using the unimodal benchmark functions

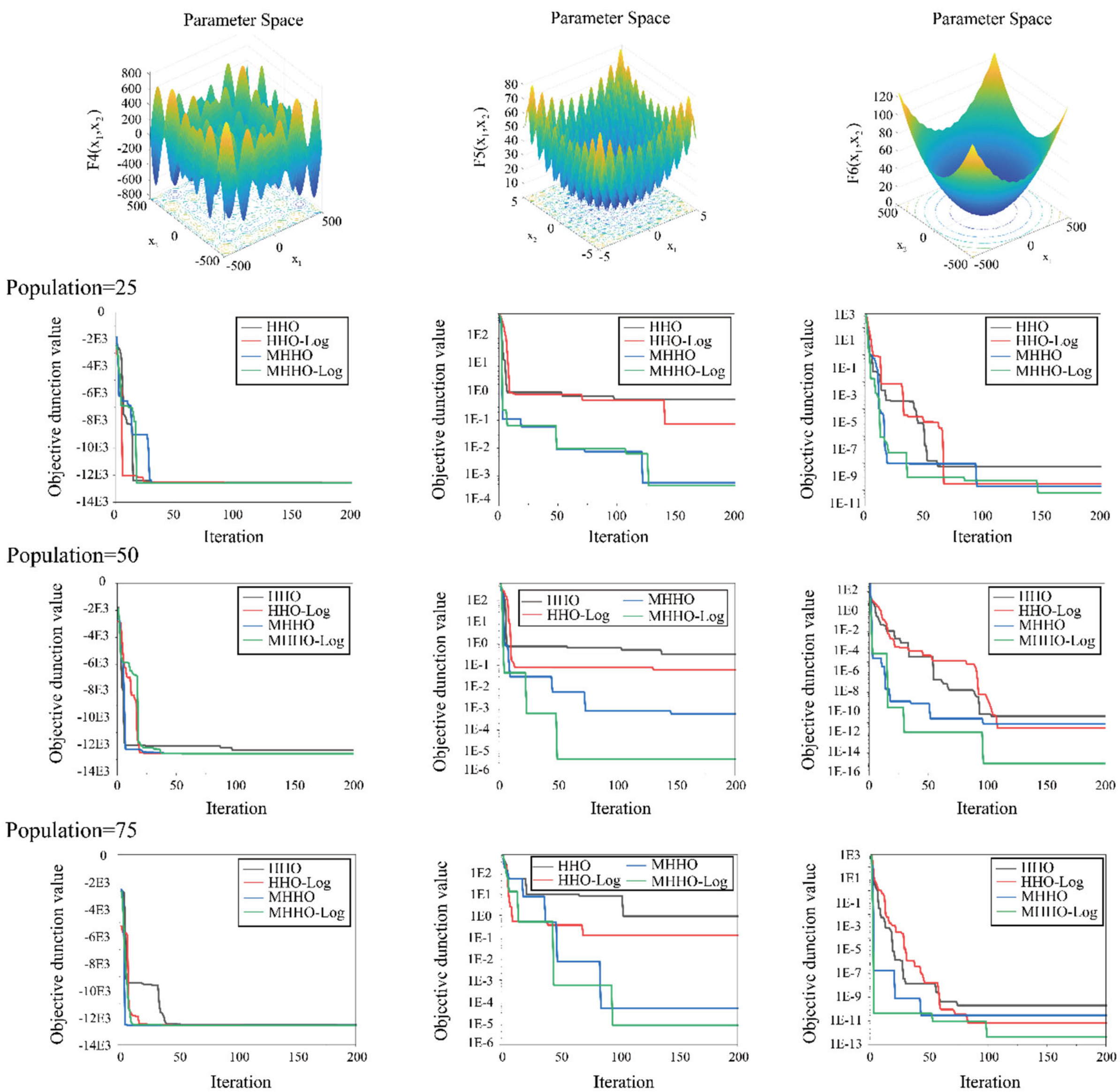

Fig. 9 Comparisons between HHO and MSHHO by using the multimodal benchmark functions

5.2 Development of MSHHO- SVR model

After verifying the performance of all MSHHO algorithms, a series of hybrid models combing MSHHO algorithms and SVR can be developed to search the optimized hyperparameters for predicting the FD. To confirm the optimization performance of MSHHO, the populations are also set equal to 25, 50 and 75 in 200 iterations, respectively. Fig. 10 displays the iteration curves of all hybrid models with the different populations. The lowest fitness value of each hybrid SVR model is obtained in the population of 50, the same as the aforementioned results in Section 5.1.

In particular, the MHHO-Log-SVR model with 50 populations has the best performance by means of the lowest value of fitness among all models. The rest of the results of the minimum values of fitness are written in Table 4. Therefore, the MHHO-Log-SVR model is considered as the optimal MSHHO model for forecasting the FD, namely the MSHHO-SVR model.

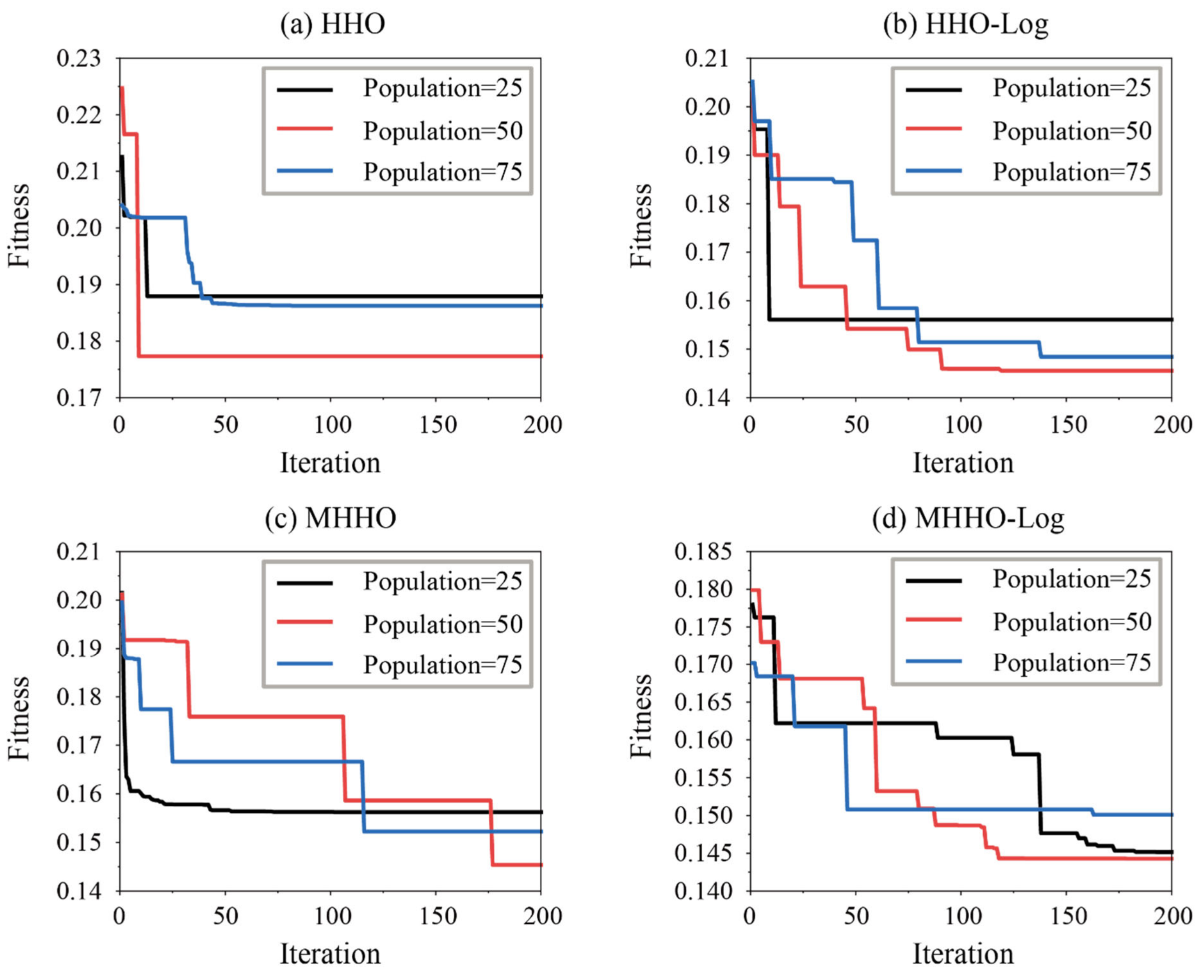

Fig. 10 Development results of HHO-SVR and MSHHO-SVR models

Table 4 Statistical analysis of fitness of all hybrid models with different populations

Models	Minimum fitness		
	Population=25	Population=50	Population=75
HHO	0.1879	0.1773	0.1862
HHO-Log	0.1561	0.1456	0.1484

MHHO	0.1562	0.1454	0.1522
MHHO-Log	**0.1452**	**0.1443**	**0.1501**

5.3 Development of ELM model

The ELM model's development solely depends on the number of neurons present in a single hidden layer (Li et al. 2022a, 2022b). In order to obtain the most accurate ELM model for estimating the FD, seven models were constructed using varying number of neurons ranging from 20 to 200. R^2 was utilized to evaluate the predictive ability of these models. The results of the seven models during both the training and testing phases have been reported in Table 5. The results indicated that increasing the number of neurons in the training phase results in an increased value of R^2. However, the 3rd ELM model achieved the highest R^2 value (0.8173) using the test data with 80 neurons in a hidden layer. Accordingly, the final ELM model with 80 neurons in a hidden layer can be employed to predict the FD in this study.

Table 5 Performance evaluation of ELM models with different number of neurons

Models No.	Neurons	R^2	
		Training phase	Testing phase
1	20	0.4188	0.2988
2	50	0.7861	0.6946
3	**80**	**0.8197**	**0.8173**
4	110	0.8812	0.6578
5	140	0.8810	0.5002
6	170	0.9051	0.4468
7	200	0.9162	0.5541

5.4 Development of KELM model

KELM model eliminates the need for selecting and determining the number of neurons in the hidden layer, instead relying on kernel function (such as the RBF) parameters to optimize the performance of the ELM model (Huang et al. 2011). Similar to the SVR model, the range of regularization coefficient (K) and γ of KELM model must be manually defined. Zhu et al. (2018) used a range of 2^{-20} to 2^{20} for K and γ. Baliarsingh et al. (2019) considered the K and γ in the range of 2^{-8} to 2^{8} to solve their problem. Therefore, the variation range of hyperparameters of KELM model is considered as 2^{-2}, 2^{-1}, …, 2^{7}, 2^{8} to predict the FD. The development results of KELM models in the training and testing phases are shown in Fig. 11. As can be shown in Fig. 11a, the R^2 has a positive relationship with K in any values of γ. However, if K is smaller than 2^1, the R^2 increases first and then decreases as γ increases, and the turning point is when $\gamma=2^1$. However, the highest value of R^2 is obtained in the testing phase when K is 2^4 and γ is 2^{-1}. As can be realized, the best hyperparameters of KELM model are 2^4 (K) and 2^{-1} (γ) for predicting the FD.

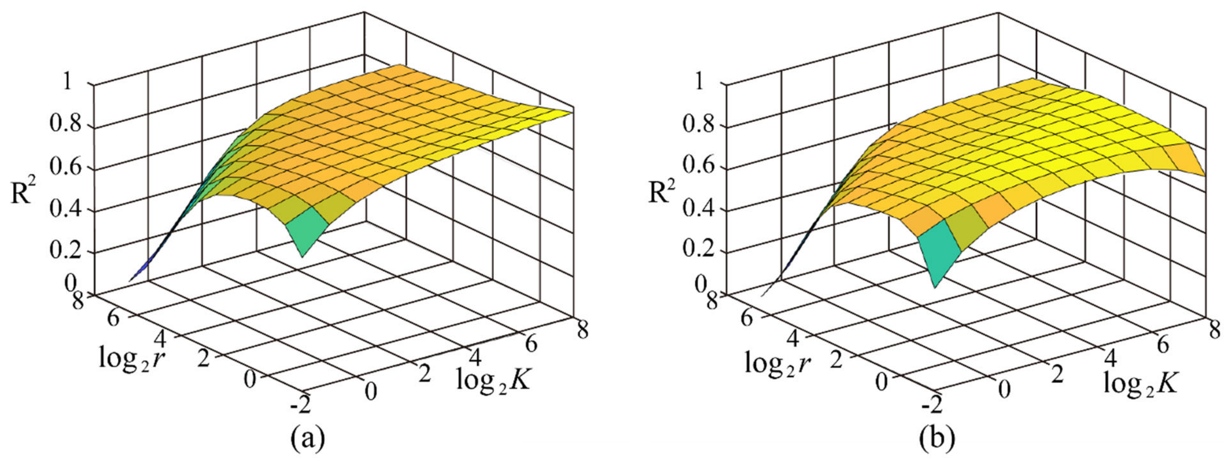

Fig. 11 Development of KELM model: (a) training phase; (b) testing phase

5.5 Development of BPNN model

BPNN model was devised with the purpose of minimizing predictive errors through the application of back-propagation to regulate the weights and biases of the neural network. This technique has gained widespread usage in addressing a range of engineering problems (Li et al. 2021a). The BPNN is also a typical multilayer neural network with input, hidden, and output layers. To develop a BPNN model, the numbers of hidden and neurons are the major concerns. Although a better performing BPNN model has more hidden layers and neurons, it may result in overfitting and increase unnecessary computation time (Yari et al. 2016). Serval formulas can be used to calculate the neurons of hidden layers (Han et al. 2018). The values of R^2 are used to describe the BPNN performance in the training and testing phases, as shown in Fig. 12a and 12b, respectively. Ultimately, the neural network model with a configuration of 6-5-4-1 (i.e., 6 neurons in the input layer, 5 neurons in the first hidden layer, 4 neurons in the second hidden layer, and 1 neuron in the output layer) achieved the highest R^2 value in the testing phase. This model was determined to be the most optimal BPNN model for predicting the FD in this study.

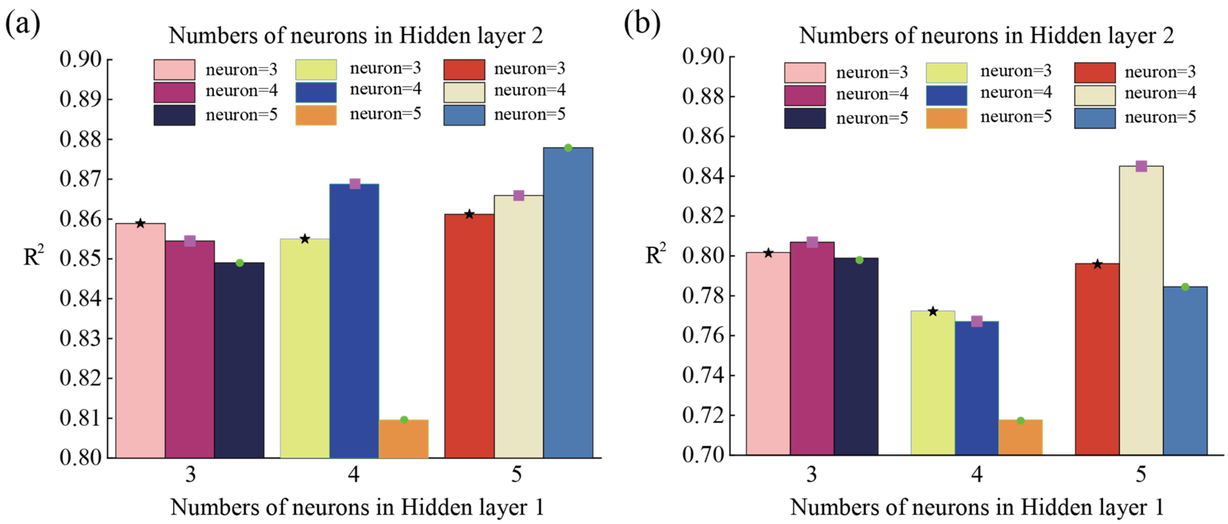

Fig. 12 Performance of the BPNN model: (a) training phase; (b) testing phase

5.6 Development of Empirical equation

There are many empirical formulas for predicting the FD by using blast design parameters (Lundborg et al. 1975; Roth 1979; Gupta 1980; Olofsson 1990). Nevertheless, the accuracy of empirical models is extremely dependent on input parameters (Richards and Moore 2004; Little 2007; Ghasemi et al. 2012; Trivedi et al. 2014). Therefore, a multiple linear regression formula was established as shown in Eq. (22), which describes the relationship between the considered six controllable parameters and FD.

$$D_{flyrock} = 0.39 \times H + 0.44 \times HD + 46.4 \times BTS - 0.27 \times ST + 0.21 \times MC + 121.65 \times PF - 31.6 \quad (22)$$

where $D_{flyrock}$ represents the FD.

6. Results and Discussion

After obtaining the ideal hyperparameters of all models, each model was run based on the same database and their prediction performances were evaluated by RMSE, R^2, MAE and VAF. Table 6 presents the performance comparison results of the proposed model and other five models in the training phase. It can be seen intuitively that the performance indices of SVR models optimized by HHO and MSHHO are obviously superior to other models. The best and worst models are the

MSHHO-SVR model and the ELM model, with RMSE of 12.2822 and 28.3539, R^2 of 0.9662 and 0.8197, MAE of 8.5034 and 21.6415, and VAF of 96.6161 % and 81.965 %, respectively. Following the MSHHO-SVR model, other models, including the HHO-SVR model, KELM model, BPNN model, and empirical equation, exhibited favorable performance based on the aforementioned evaluation metrics for predicting the FD.

Table 6 Comparison of the performance of models (in the training phase)

Models	Performance			
	RMSE	R^2	MAE	VAF (%)
HHO-SVR	17.5967	0.9305	10.3371	93.1426
MSHHO-SVR	**12.2822**	**0.9662**	**8.5034**	**96.6161**
ELM	28.3539	0.8197	21.6415	81.9652
KELM	19.3470	0.9160	13.6868	91.6069
BPNN	24.4488	0.8659	18.0935	86.5910
Empirical	27.6668	0.8283	20.8974	82.8521

The regression diagrams were used to evaluate the performance of the six models in the training phase as shown in Fig. 13. The horizontal axis represents the observed FD values, while the predicted values are listed on the vertical axis. Each diagram includes a line at 45°, which is colored differently for each model (black, red, green, yellow, purple, and blue). The points on these lines indicate that the error between the predicted and the observed values is zero. A greater number of points on or close to the line of 45° indicates that the model has better predictive accuracy. Meanwhile, the dotted lines with the equation of y=1.1x and y=0.9x were set as the prediction boundaries, and those points outside these boundaries have the lowest performance. As can be seen in this picture, the predicted values by MSHHO-SVR model are more concentrated on the color line of 45, followed by HHO-SVR model, KELM model, BPNN model, empirical and ELM model. Meanwhile, it can be seen that the MSHHO-SVR model has better performance indices than other models.

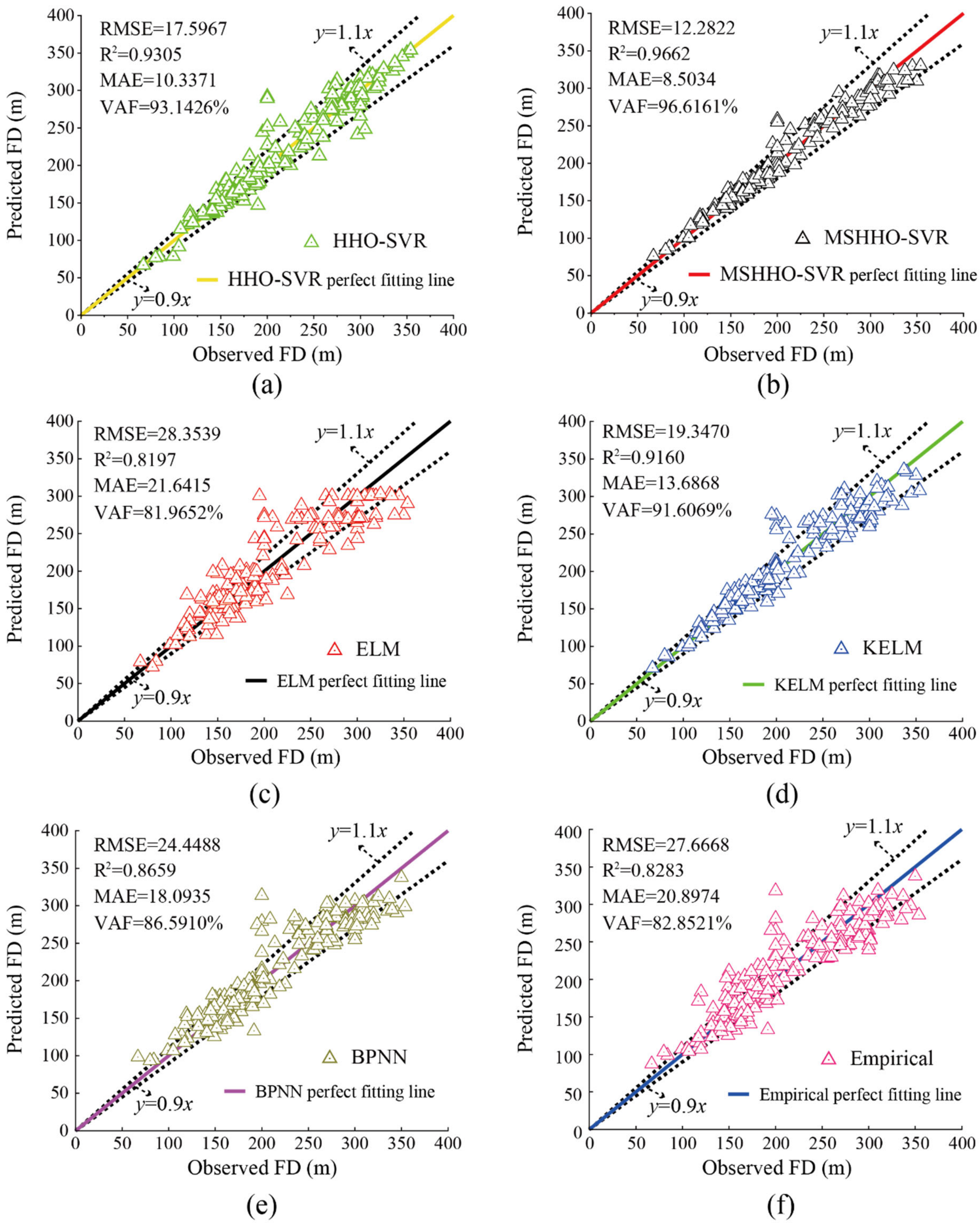

Fig. 13 Regression diagrams of all models using the training set: (a) HHO-SVR; (b) MSHHO-SVR; (c) ELM; (d) KELM (e) BPNN; (f) Empirical

It is worth noting that a model that performs well in the training phase cannot be directly applied to predict the FD. In order to verify their efficacy, the proposed model, along with five others, should undergo validation using the test set. It is important to note that the models may not necessarily reproduce the same luminous results in the testing phase. Table 7 displays the results of the four performance indices generated by all the models. The MSHHO-SVR model emerges as the most effective among them, yielding the highest values of R^2 value (0.9691) and VAF (96.9178%), as well as the lowest values of RMSE (9.6685) and MAE (7.4618). Conversely, the empirical model displays poor prediction accuracy with an RMSE value of 26.4389, R^2 value of 0.7689, MAE value of 20.4681, and VAF value of 76.9583%. Furthermore, the empirical equation also generates predictive values that deviate significantly from the 45° color line. Conversely, the MSHHO-SVR model's prediction performance is the most superior, as demonstrated in Fig. 14, where all the predicted values fall within the prediction boundary and are positioned closer to the 45° color line. The HHO-SVR model, followed by the BPNN model and the KELM model, perform less effectively than the MSHHO-SVR model in the FD prediction.

Table 7 Comparison of the performance of models (in the testing phase)

Models	Performance			
	RMSE	R^2	MAE	VAF (%)
HHO-SVR	13.9193	0.9359	8.5762	93.6147
MSHHO-SVR	**9.6685**	**0.9691**	**7.4618**	**96.9178**
ELM	23.5062	0.8173	18.3581	82.5412
KELM	22.5800	0.8314	15.9271	83.3616
BPNN	21.6496	0.8450	15.5799	84.5856
Empirical	26.4389	0.7689	20.4681	76.9583

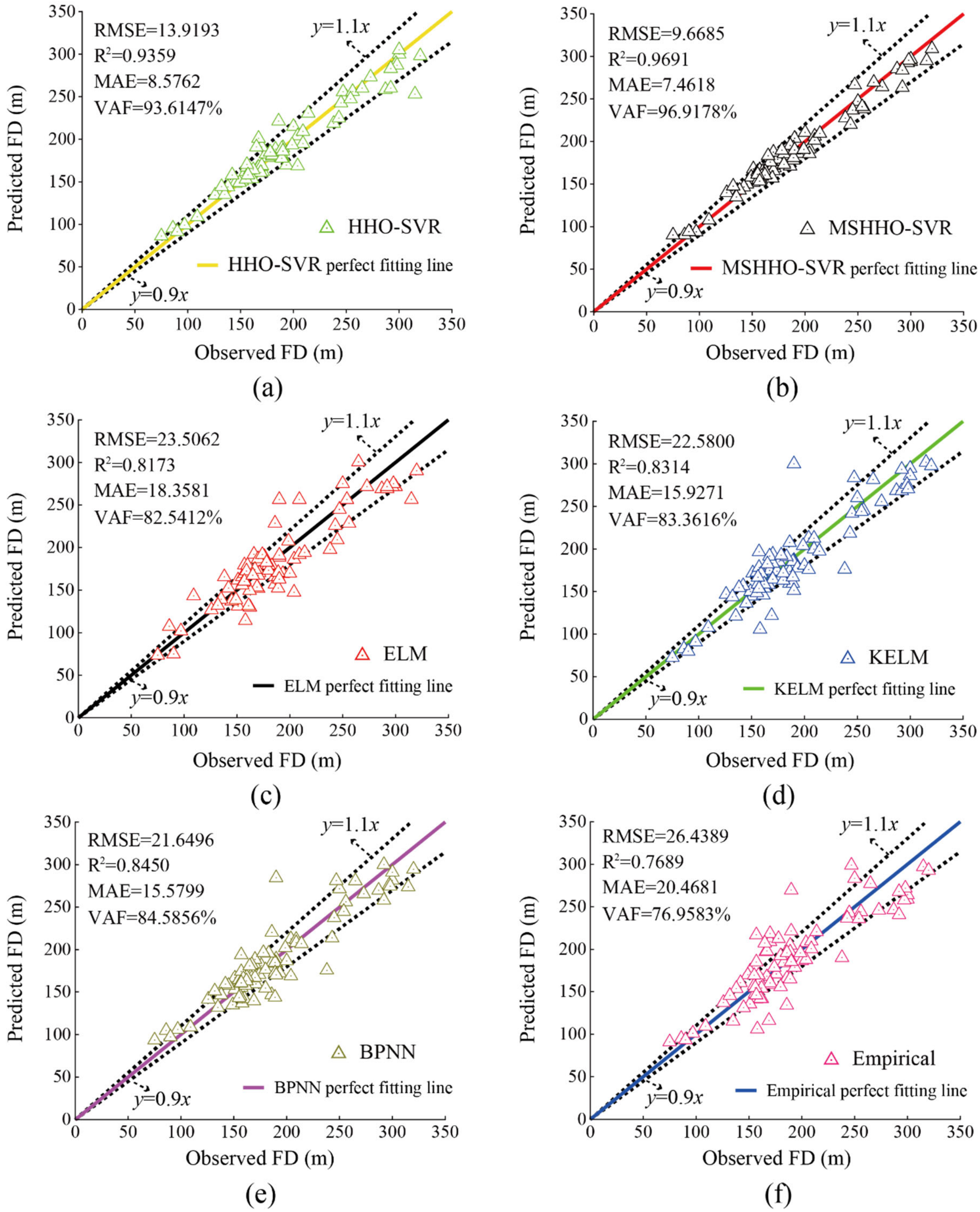

Fig. 14 Regression diagrams of all models using the test set: (a) HHO-SVR; (b) MSHHO-SVR; (c) ELM; (d) KELM (e) BPNN; (f) Empirical

Fig. 15 presents the graphical Taylor diagrams that comprehensively compare the predictive performance of all models in both the training and testing phases. The horizontal and vertical axes represent St. D of predicted values based various models, which are draw by blue circular lines. The green circles in these diagrams represent the RMSE of different models, and the black line from the origin (0, 0) to the outermost circle shows the R in the range of 0 to 1. In the Taylor diagrams, the RMSE and R of observed value are set by default to 0 and 1, respectively. The St. D values can be calculated from the raw data of the training and test sets. Then, the positions of all models can be determined according to the values of St. D, RMSE, and R from the respective prediction results. Accordingly, the best model has a less movement to the observed value than any other model. As can be seen in these diagrams, the MSHHO-SVR model is certainly closer to the observed value in both the training and testing phases, which indicates the best model is the MSHHO-SVR model for predicting the FD.

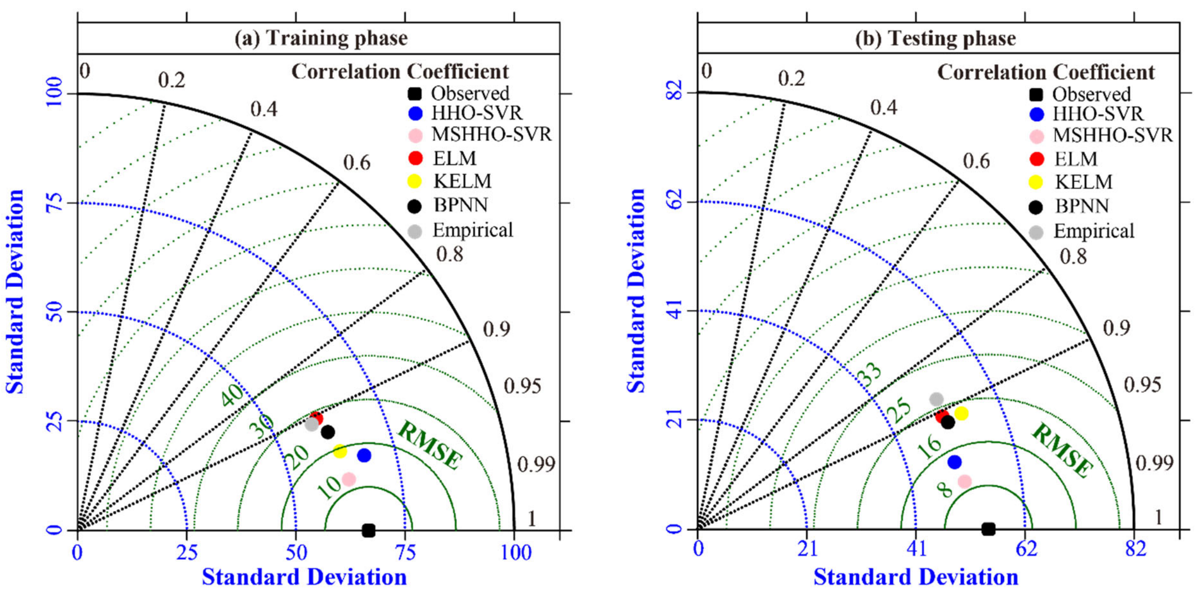

Fig. 15 Graphical Taylor diagrams for comparison of all models

Fig. 16 illustrates the curves of both observed and predicted FD using the test set, enabling a detailed assessment of the predictive performance of the six models. On the whole, there is little difference between the predicted and observed curves of all models. However, local observation shows that the predicted values by empirical models have a large error from the observed values of No.33-35 samples, the errors obtained by ELM, KELM, and BPNN models are almost the same but obviously larger than that obtained by HHO-SVR model. Compared to the HHO-SVR model, there is little error between the predicted and observed values of No. 20 to No. 30 samples based on the MSHHO-SVR model, which means that the MSHHO-SVR model is more suitable for predicting the FD than other models by means of higher prediction accuracy.

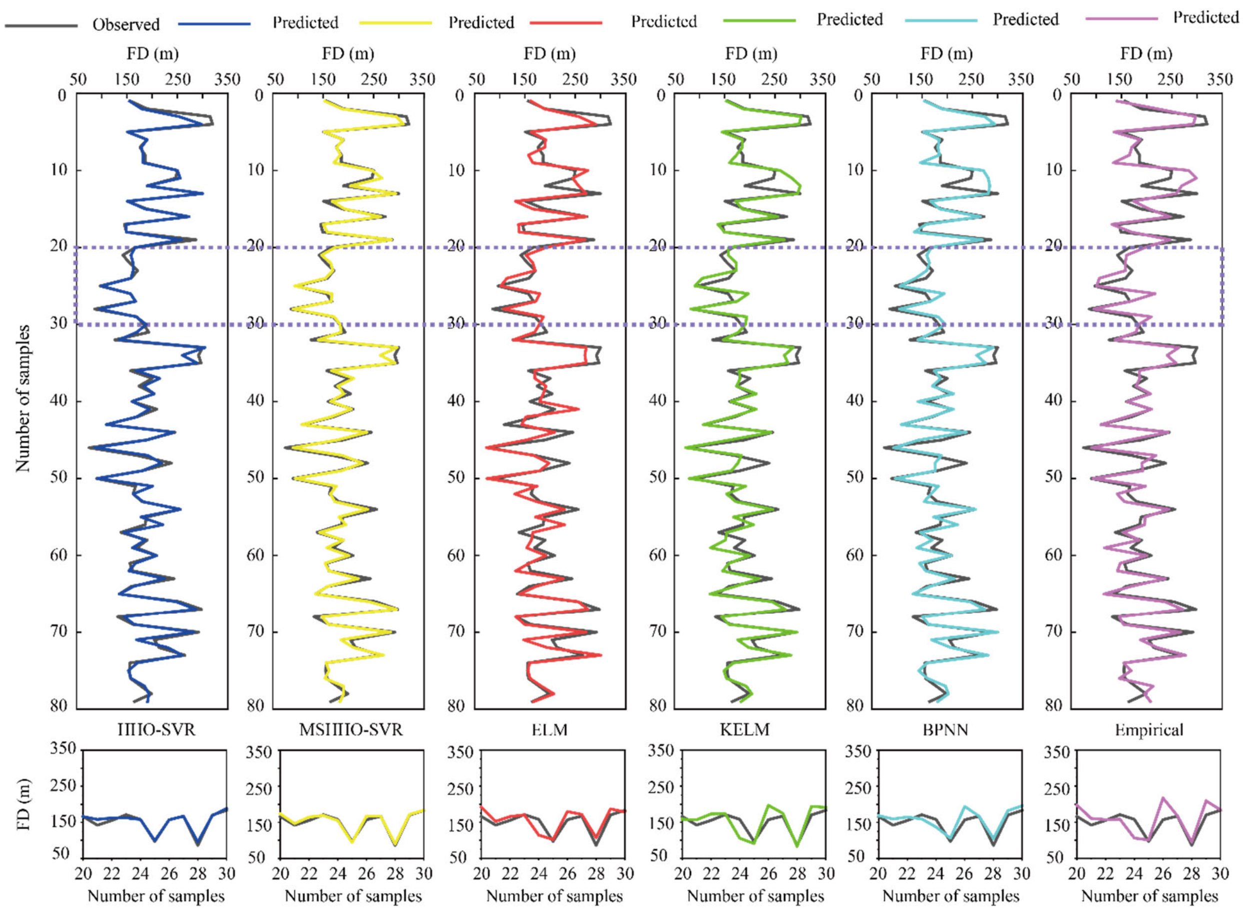

Fig. 16 The curves of predicting FD in the testing phase by all models

In order to further compare prediction performance between the HHO-SVR model and the MSHHO-SVR model, the relative deviation is defined to measure the difference in prediction performance of the proposed models in the training and testing phases, respectively. If the relative deviation is greater than 10% or less than -10%, the prediction is considered wrong. According to the obtained results as shown in Fig. 17, the relative deviation of the MSHHO-SVR model is more concentrated in [-10%, 10%] than the HHO-SVR model in both of the training and testing phases. This is strong evidence that MSHHO can help SVR do a much better job of predicting the FD.

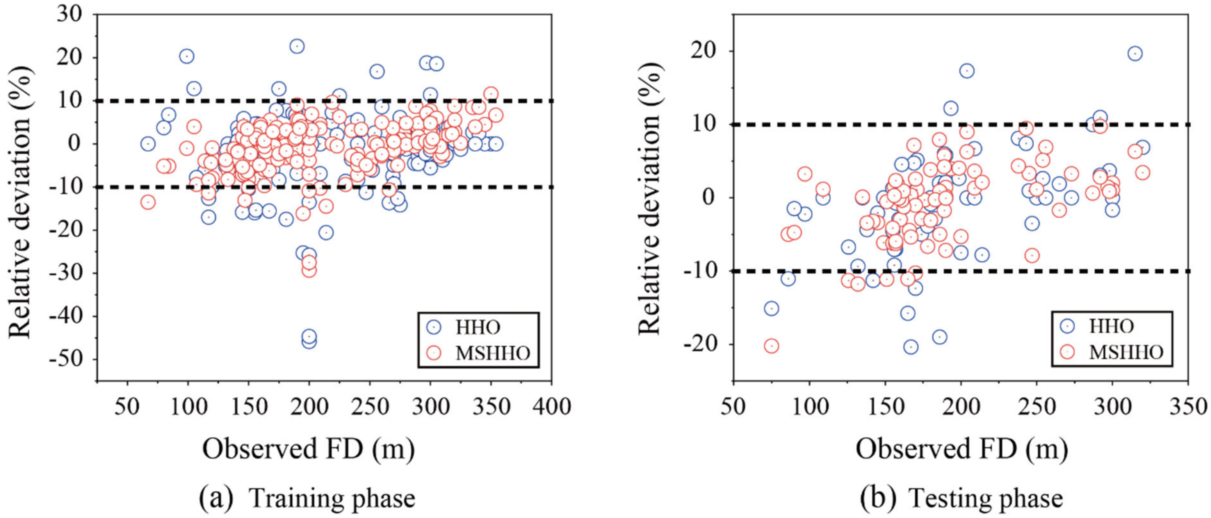

Fig. 17 Variation of the relative deviation for evaluating the performance of HHO-SVR and MSHHO-SVR mode

Although six controllable parameters related to the blasting design are considered as input parameters in this study, the importance of them still needs to be checked using the MSHHO-SVR model. The SHAP method inspired by cooperative game theories has been widely used to calculate the parameter importance (Lundberg and Lee 2017). The result of the importance scores obtained by mean SHAP values is shown in Fig. 18. As can be seen in this figure, the order of parameter importance is H, PF, MC, HD, ST, and BTS with mean SHAP values of 40.25, 19.98, 10, 3.81, 3.76, and 2.81, respectively. The biggest advantage of the SHAP method is that the influence of features can be reflected in each sample, which also shows the positive and negative influence. Fig. 19 displays the influence of each parameter on FD prediction. In this picture, the overlap points depict the SHAP value distribution for each parameter. The higher the positive or negative SHAP values, the greater the impact on FD prediction. The influence results illustrate that the FD significantly increases with H and PF. Meanwhile, all input parameters are positively correlated with the FD.

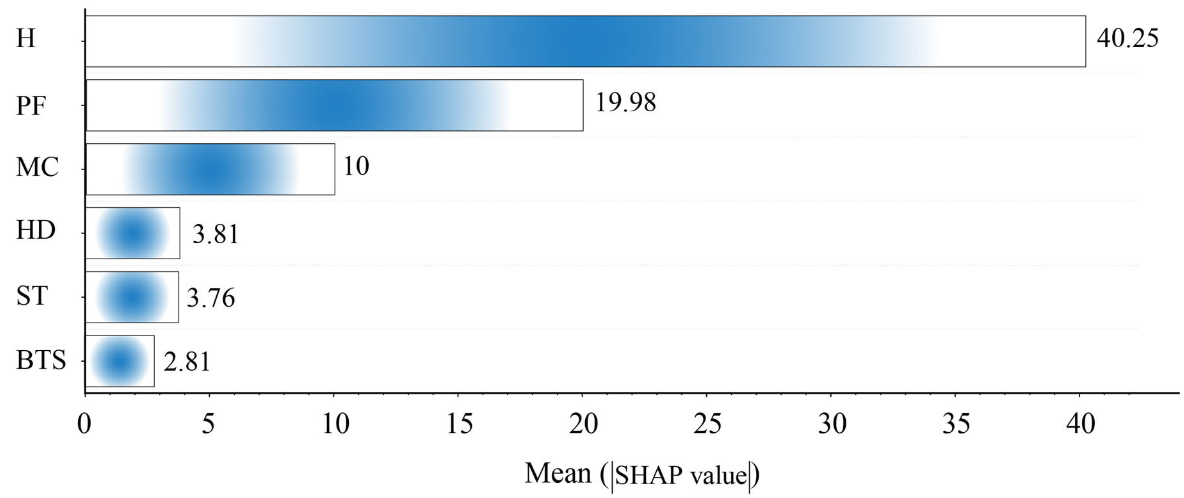

Fig. 18 Importance scores of input parameters

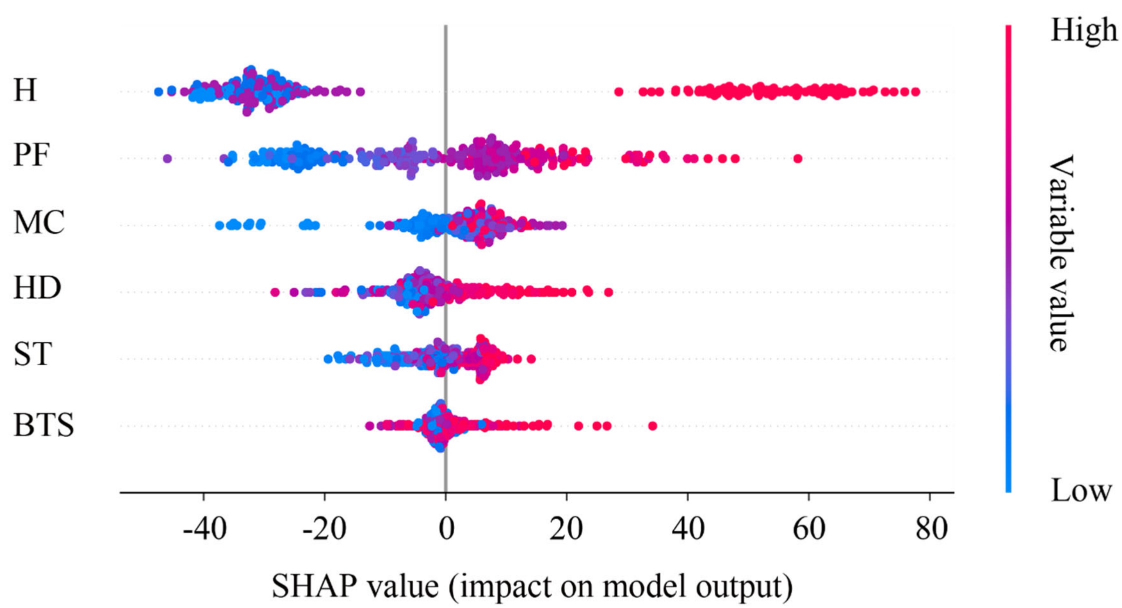

Fig. 19 Influence results of each parameter on FD prediction

In this study, the MSHHO-SVR model has confirmed as the effective model to predict the FD with an excellent performance, which is similar with most of published hybrid models from 2012-2022 as shown in Table 8. It can be seen that the best model was HHO-MLP proposed by Murlidhar et al. (2021) by means of the highest value of R^2 (0.998). However, the difference in the used number of samples in database and considered input parameters is the root cause of the difference in model performance. Based on the same data set considered in this study, Ye et al. (2021) developed genetic programming (GP) and RF models to predict the FD with good prediction accuracy of R^2 are 0.908 and 0.9046, respectively; Armaghani et al. (2020) proposed a SVR model to estimate the FD with high accuracy (R^2= 0.9373); Murlidhar et al. (2020) used biogeography-based optimization (BBO) to optimize the ELM model for predicting the FD, with R^2= 0.94. The current study has yielded superior results for predicting the FD, as determined by the use of the most effective model, the MSHHO-SVR, which yielded higher R^2 values (0.9662 for the training set and 0.9691 for the test set). Therefore, the authors are confident that the proposed MSHHO-SVR model exhibits superior performance compared to the existing models on the same dataset.

Table 8 Comparison of the proposed models with other hybrid models in FD prediction.

References	Models	Input	Data set no.	Performance
Monjezi et al. (2012)	GA-ANN	B, S, HD, ST, SD, PF, MC, RMR	195	R^2=0.976
Armaghani et al. (2014)	PSO-ANN	B, PF, SD, MC, H, S, ST, N, RD	44	R^2=0.930
Koopialipoor et al. (2019)	ICA-ANN PSO-ANN GA-ANN	BTS, H, PF, MC, HD, ST	262	$R^2_{ICA\text{-}ANN}$=0.958 $R^2_{ICA\text{-}ANN}$=0.959 $R^2_{ICA\text{-}ANN}$=0.932
Kalaivaani et al. (2020)	PSO-RFNN	B, S, ST, MC	72	R^2=0.933
Hasanipanah et al. (2020)	HS-ANN PSO-ANN ADHS-ANN	S, B, ST, PF, r	82	$R^2_{HS\text{-}ANN}$=0.871 $R^2_{PSO\text{-}ANN}$=0.832 $R^2_{ADHS\text{-}ANN}$=0.929
Nikafshan Rad et al. (2020)	GA-RFNN	S, B, ST, MC	70	R^2=0.9667
Li et al. (2021f)	GA-ANN PSO-ANN ICA-ANN ABC-ANN	BTS, HD, ST, MC, PF, RD, Rn	113	$R^2_{GA\text{-}ANN}$=0.9466 $R^2_{PSO\text{-}ANN}$=0.9608 $R^2_{ICA\text{-}ANN}$=0.9598 $R^2_{ABC\text{-}ANN}$=0.9666

	FA-ANN			R^2_{FA-ANN}=0.9719
Murlidhar et al. (2020)	PSO-ELM BBO-ELM	BTS, H, PF, ST, MC, HD	262	$R^2_{PSO-ELM}$=0.93 $R^2_{BBO-ELM}$=0.94
Murlidhar et al. (2021)	HHO-MLP	H, ST/B, HD, CPM, PF, GSI, RQD, WI	152	$R^2_{HHO-MLP}$=0.998
Nguyen et al. (2021)	WOA-SVM	B, S, ST, PF, W	210	R^2=0.977
Fattahi and Hasanipanah (2022)	GOA-ANFIS CA- ANFIS	S, B, ST, PF, RD	80	$R^2_{GOA-ANFIS}$=0.974 $R^2_{CA-ANFIS}$=0.953
This study	HHO-SVR MSHHO-SVR	BTS, H, PF, ST, MC, HD	262	$R^2_{HHO-SVR}$=0.9359 $R^2_{MSHHO-SVR}$=0.9691

Note: r= density of rock; RFNN-Recurrent fuzzy neural network; MLP-Multi-layer perceptron; BBO-Biogeography-based optimization; HS-Harmony search; CA-Cultural algorithm; ICA-Imperialist competitive algorithm; ACO-Ant colony optimization; ADHS-Adaptive dynamical harmony search; ABC-Artificial bee colony.

7. Conclusion

Flyrock has long been a significant safety concern in open-pit mines. This study examines a rich database from six open pit mines in Malaysia, comprising 262 blasting operations. A novel optimization model combining HHO and MS was developed to fine-tune the SVR model, named the MSHHO-SVR model. This model was compared the predictive performance with other models, including the HHO-SVR, ELM, KELM, BPNN, and empirical models for predicting the FD. Then, the main conclusions of this study are listed as follows:

(1) Evaluation results indicated that the MSHHO-SVR model has the highest predictive accuracy among all models, as reflected by its RMSE values of 12.2822 and 9.6685, R^2 values of 0.9662 and 0.9691, MAE values of 8.5034 and 7.4618, and VAF values of 96.6161% and 96.9178% in the training and testing phases, respectively.

(2) It is verified that multi-strategies can significantly improve the performance of the HHO algorithm for tunning the hyperparameters of the SVR model. Furthermore, the combination of MSHHO and SVR model has a superior prediction accuracy than precious developed models using the same FD database.

(3) The result of sensitivity analysis showed that the H is the most sensitive and the BTS is the least sensitive parameter to FD, respectively. The importance ranking of rest input parameters is

PF, MC, HD, and ST. Noted that all input parameters are positively correlated with the FD, especially the H and PF.

Although the proposed novel hybrid model is able to predict the FD with a satisfactory predictive accuracy, if the range of input parameter values extends beyond those employed in this study, the findings may be subject to bias. Therefore, it is necessary to obtain more data from field investigation and inspection to enrich the database and improve the model generalization. Furthermore, some physics rules between input parameters and the model output could be included in future flyrock studies. In this regard, predicted FD by using previous empirical formulas can be considered as model inputs. This idea might be more interesting for mining and civil engineers because they can learn more about how data is prepared and how input and output parameters are related.

Declaration of Competing Interests

The authors declare that they have no known competing financial interests or personal relationships that could have appeared to influence the work reported in this paper.

Acknowledgements

This research is partially supported by the National Natural Science Foundation Project of China (42177164), and the Innovation-Driven Project of Central South University (2020CX040). The first author was funded by China Scholarship Council (Grant No. 202106370038).

References

Adnan, R. M., Meshram, S. G., Mostafa, R. R., Islam, A. R. M. T., Abba, S. I., Andorful, F., & Chen, Z. (2023b). Application of Advanced Optimized Soft Computing Models for Atmospheric Variable Forecasting. Mathematics, 11(5), 1213.

Adnan, R. M., Mostafa, R. R., Dai, H. L., Heddam, S., Kuriqi, A., & Kisi, O. (2023a). Pan evaporation estimation by relevance vector machine tuned with new metaheuristic algorithms using limited climatic data. Engineering Applications of Computational Fluid Mechanics, 17(1), 2192258.

Armaghani, D. J., Hajihassani, M., Mohamad, E. T., Marto, A., & Noorani, S. A. (2014). Blasting-induced flyrock and ground vibration prediction through an expert artificial neural network based on particle swarm optimization. Arabian Journal of Geosciences, 7(12), 5383-5396.

Armaghani, D. J., Harandizadeh, H., Momeni, E., Maizir, H., & Zhou, J. (2021). An optimized system of GMDH-ANFIS predictive model by ICA for estimating pile bearing capacity. Artificial Intelligence Review, 1-38.

Armaghani, D. J., Koopialipoor, M., Bahri, M., Hasanipanah, M., & Tahir, M. M. (2020). A SVR-GWO technique to minimize flyrock distance resulting from blasting. Bulletin of Engineering Geology and the Environment, 79(8), 4369-4385.

Armaghani, D. J., Mohamad, E. T., Hajihassani, M., Abad, S. A. N. K., Marto, A., & Moghaddam, M. R. (2016). Evaluation and prediction of flyrock resulting from blasting operations using empirical and computational methods. Engineering with Computers, 32(1), 109–121.

Asl, P. F., Monjezi, M., Hamidi, J. K., & Armaghani, D. J. (2018). Optimization of flyrock and rock fragmentation in the Tajareh limestone mine using metaheuristics method of firefly algorithm. Engineering with Computers, 34(2), 241-251.

Bagchi A, Gupta RN (1990) Surface blasting and its impact on environmental. In: Workshop on Environmental Management of Mining Operations, Varanasi, pp 262–279.

Bajpayee TS, Rehak TR, Mowrey GL, Ingram DK (2004) Blasting injuries in surface mining with emphasis on flyrock and blast area security. J Saf Res 35(1):47–57.

Bakhtavar, E., Nourizadeh, H., & Sahebi, A. A. (2017). Toward predicting blast-induced flyrock: a hybrid dimensional analysis fuzzy inference system. International journal of environmental science and technology, 14, 717-728.

Baliarsingh, S. K., Vipsita, S., Muhammad, K., Dash, B., & Bakshi, S. (2019). Analysis of high-dimensional genomic data employing a novel bio-inspired algorithm. Applied Soft Computing, 77, 520-532.

Chen, D. F., Feng, X. T., Xu, D. P., Jiang, Q., Yang, C. X., & Yao, P. P. (2016). Use of an improved ANN model to predict collapse depth of thin and extremely thin layered rock strata during tunnelling. Tunnelling and Underground Space Technology, 51, 372-386.

Dai, Y., Khandelwal, M., Qiu, Y., Zhou, J., Monjezi, M., & Yang, P. (2022). A hybrid metaheuristic approach using random forest and particle swarm optimization to study and evaluate backbreak in open-pit blasting. Neural Computing and Applications, 1-16.

Du, K., Liu, M., Zhou, J., & Khandelwal, M. (2022). Investigating the Slurry Fluidity and Strength Characteristics of Cemented Backfill and Strength Prediction Models by Developing Hybrid GA-SVR and PSO-SVR. Mining, Metallurgy & Exploration, 1-20.

Elgamal, Z. M., Yasin, N. B. M., Tubishat, M., Alswaitti, M., & Mirjalili, S. (2020). An improved harris hawks optimization algorithm with simulated annealing for feature selection in the medical field. IEEE Access, 8, 186638-186652.

Elkatatny, S., Mahmoud, M., Tariq, Z., & Abdulraheem, A. (2018). New insights into the prediction of heterogeneous carbonate reservoir permeability from well logs using artificial intelligence network. Neural Computing and Applications, 30(9), 2673-2683.

Fan, Q., Chen, Z., & Xia, Z. (2020). A novel quasi-reflected Harris hawks optimization algorithm for global optimization problems. Soft Computing, 24(19), 14825-14843.

Faradonbeh, R. S., Jahed Armaghani, D., & Monjezi, M. (2016). Development of a new model for predicting flyrock distance in quarry blasting: a genetic programming technique. Bulletin of Engineering Geology and the Environment, 75(3), 993-1006.

Fattahi, H., & Hasanipanah, M. (2022). An integrated approach of ANFIS-grasshopper optimization algorithm to approximate flyrock distance in mine blasting. Engineering with Computers, 1-13.

Ghaleini, E. N., Koopialipoor, M., Momenzadeh, M., Sarafraz, M. E., Mohamad, E. T., & Gordan, B. (2019). A combination of artificial bee colony and neural network for approximating the safety factor of retaining walls. Engineering with Computers, 35(2), 647-658.

Ghasemi, E., Sari, M., & Ataei, M. (2012). Development of an empirical model for predicting the effects of controllable blasting parameters on flyrock distance in surface mines. International Journal of Rock Mechanics and Mining Sciences, 52, 163-170.

Guo, H., Nguyen, H., Bui, X. N., & Armaghani, D. J. (2021b). A new technique to predict fly-rock in bench blasting based on an ensemble of support vector regression and GLMNET. Engineering with Computers, 37(1), 421-435.

Guo, H., Zhou, J., Koopialipoor, M., Jahed Armaghani, D., & Tahir, M. M. (2021a). Deep neural network and whale optimization algorithm to assess flyrock induced by blasting. Engineering with Computers, 37(1), 173-186.

Han, H., Jahed Armaghani, D., Tarinejad, R., Zhou, J., & Tahir, M. M. (2020). Random forest and bayesian network techniques for probabilistic prediction of flyrock induced by blasting in quarry sites. Natural Resources Research, 29(2), 655-667.

Han, L., Fuqiang, L., Zheng, D., & Weixu, X. (2018). A lithology identification method for continental shale oil reservoir based on BP neural network. Journal of Geophysics and Engineering, 15(3), 895-908.

Hasanipanah, M., Amnieh, H. B., Arab, H., & Zamzam, M. S. (2018b). Feasibility of PSO–ANFIS model to estimate rock fragmentation produced by mine blasting. Neural Computing and Applications, 30, 1015-1024.

Hasanipanah, M., Jahed Armaghani, D., Bakhshandeh Amnieh, H., Koopialipoor, M., & Arab, H. (2018a). A risk-based technique to analyze flyrock results through rock engineering system. Geotechnical and Geological Engineering, 36(4), 2247-2260.

Hasanipanah, M., Jahed Armaghani, D., Bakhshandeh Amnieh, H., Majid, M. Z. A., & Tahir, M. (2017). Application of PSO to develop a powerful equation for prediction of flyrock due to blasting. Neural Computing and Applications, 28(1), 1043-1050.

Hasanipanah, M., Keshtegar, B., Thai, D. K., & Troung, N. T. (2020). An ANN-adaptive dynamical harmony search algorithm to approximate the flyrock resulting from blasting. Engineering with Computers, 1-13.

Hasanipanah, M., Monjezi, M., Shahnazar, A., Armaghani, D. J., & Farazmand, A. (2015). Feasibility of indirect determination of blast induced ground vibration based on support vector machine. Measurement, 75, 289-297.

Hasanipanah, M., Noorian-Bidgoli, M., Jahed Armaghani, D., & Khamesi, H. (2016). Feasibility of PSO-ANN model for predicting surface settlement caused by tunneling. Engineering with Computers, 32, 705-715.

Heidari, A. A., Mirjalili, S., Faris, H., Aljarah, I., Mafarja, M., & Chen, H. (2019). Harris hawks optimization: Algorithm and applications. Future generation computer systems, 97, 849-872.

Hosseini, S., Lawal, A. I., & Kwon, S. (2023). A causality-weighted approach for prioritizing mining 4.0 strategies integrating reliability-based fuzzy cognitive map and hybrid decision-making methods: A case study of Nigerian Mining Sector. Resources Policy, 82, 103426.

Hosseini, S., Poormirzaee, R., & Hajihassani, M. (2022a). An uncertainty hybrid model for risk assessment and prediction of blast-induced rock mass fragmentation. International Journal of Rock Mechanics and Mining Sciences, 160, 105250.

Hosseini, S., Poormirzaee, R., & Hajihassani, M. (2022b). Application of reliability-based back-propagation causality-weighted neural networks to estimate air-overpressure due to mine blasting. Engineering Applications of Artificial Intelligence, 115, 105281.

Hosseini, S., Poormirzaee, R., Hajihassani, M., & Kalatehjari, R. (2022). An ANN-fuzzy cognitive map-based Z-number theory to predict flyrock induced by blasting in open-pit mines. Rock Mechanics and Rock Engineering, 55(7), 4373-4390.

Huang, G. B., Zhou, H., Ding, X., & Zhang, R. (2011). Extreme learning machine for regression and multiclass classification. IEEE Transactions on Systems, Man, and Cybernetics, Part B (Cybernetics), 42(2), 513-529.

Huang, G. B., Zhu, Q. Y., & Siew, C. K. (2006). Extreme learning machine: theory and applications. Neurocomputing, 70(1-3), 489-501.

Hudaverdi, T., & Akyildiz, O. (2019). A new classification approach for prediction of flyrock throw in surface mines. Bulletin of Engineering Geology and the Environment, 78(1), 177-187.

Hussain, K., Neggaz, N., Zhu, W., & Houssein, E. H. (2021). An efficient hybrid sine-cosine Harris hawks optimization for low and high-dimensional feature selection. Expert Systems with Applications, 176, 114778.

Hussien, A. G., & Amin, M. (2022). A self-adaptive Harris Hawks optimization algorithm with opposition-based learning and chaotic local search strategy for global optimization and feature selection. International Journal of Machine Learning and Cybernetics, 13(2), 309-336.

Ikram, R. M. A., Dai, H. L., Al-Bahrani, M., & Mamlooki, M. (2022b). Prediction of the FRP Reinforced Concrete Beam shear capacity by using ELM-CRFOA. Measurement, 205, 112230.

Ikram, R. M. A., Hazarika, B. B., Gupta, D., Heddam, S., & Kisi, O. (2023b). Streamflow prediction in mountainous region using new machine learning and data preprocessing methods: A case study. Neural Computing and Applications, 35(12), 9053-9070.

Ikram, R. M. A., Mostafa, R. R., Chen, Z., Islam, A. R. M. T., Kisi, O., Kuriqi, A., & Zounemat-Kermani, M. (2022a). Advanced Hybrid Metaheuristic Machine Learning Models Application for Reference Crop Evapotranspiration Prediction. Agronomy, 13(1), 98.

Ikram, R. M. A., Mostafa, R. R., Chen, Z., Parmar, K. S., Kisi, O., & Zounemat-Kermani, M. (2023a). Water temperature prediction using improved deep learning methods through reptile search algorithm and weighted mean of vectors optimizer. Journal of Marine Science and Engineering, 11(2), 259.

Jamei, M., Hasanipanah, M., Karbasi, M., Ahmadianfar, I., & Taherifar, S. (2021). Prediction of flyrock induced by mine blasting using a novel kernel-based extreme learning machine. Journal of Rock Mechanics and Geotechnical Engineering, 13(6), 1438-1451.

Kalaivaani, P. T., Akila, T., Tahir, M. M., Ahmed, M., & Surendar, A. (2020). A novel intelligent approach to simulate the blast-induced flyrock based on RFNN combined with PSO. Engineering with Computers, 36(2), 435-442.

Kardani, N., Bardhan, A., Roy, B., Samui, P., Nazem, M., Armaghani, D. J., & Zhou, A. (2021). A novel improved Harris Hawks optimization algorithm coupled with ELM for predicting permeability of tight carbonates. Engineering with Computers, 1-24.

Kaveh, A., Rahmani, P., & Eslamlou, A. D. (2022). An efficient hybrid approach based on Harris Hawks optimization and imperialist competitive algorithm for structural optimization. Engineering with Computers, 38(2), 1555-1583.

Khandelwal, M., & Singh, T. N. (2005). Prediction of blast induced air overpressure in opencast mine. Noise & Vibration Worldwide, 36(2), 7-16.

Khatibinia, M., & Khosravi, S. (2014). A hybrid approach based on an improved gravitational search algorithm and orthogonal crossover for optimal shape design of concrete gravity dams. Applied Soft Computing, 16, 223-233.

Kohli, M., & Arora, S. (2018). Chaotic grey wolf optimization algorithm for constrained optimization problems. Journal of computational design and engineering, 5(4), 458-472.

Koopialipoor, M., Fallah, A., Armaghani, D. J., Azizi, A., & Mohamad, E. T. (2019). Three hybrid intelligent models in estimating flyrock distance resulting from blasting. Engineering with Computers, 35(1), 243-256.

Kumar, N., Mishra, B., & Bali, V. (2018). A novel approach for blast-induced fly rock prediction based on particle swarm optimization and artificial neural network. In Proceedings of International Conference on Recent Advancement on Computer and Communication (pp. 19-27). Springer, Singapore.

Li, C., Li, J., Chen, H., Jin, M., & Ren, H. (2021c). Enhanced Harris hawks optimization with multi-strategy for global optimization tasks. Expert Systems with Applications, 185, 115499.

Li, C., Zhou, J., Armaghani, D. J., & Li, X. (2021a). Stability analysis of underground mine hard rock pillars via combination of finite difference methods, neural networks, and Monte Carlo simulation techniques. Underground Space, 6(4), 379-395.

Li, C., Zhou, J., Armaghani, D. J., Cao, W., & Yagiz, S. (2021b). Stochastic assessment of hard rock pillar stability based on the geological strength index system. Geomechanics and Geophysics for Geo-Energy and Geo-Resources, 7(2), 1-24.

Li, C., Zhou, J., Dias, D., & Gui, Y. (2022c). A Kernel Extreme Learning Machine-Grey Wolf Optimizer (KELM-GWO) Model to Predict Uniaxial Compressive Strength of Rock. Applied Sciences, 12(17), 8468.

Li, C., Zhou, J., Khandelwal, M., Zhang, X., Monjezi, M., & Qiu, Y. (2022a). Six Novel Hybrid Extreme Learning Machine–Swarm Intelligence Optimization (ELM–SIO) Models for Predicting Backbreak in Open-Pit Blasting. Natural Resources Research, 1-23.

Li, C., Zhou, J., Tao, M., Du, K., Wang, S., Armaghani, D. J., & Mohamad, E. T. (2022b). Developing hybrid ELM-ALO, ELM-LSO and ELM-SOA models for predicting advance rate of TBM. Transportation Geotechnics, 100819.

Li, D., Koopialipoor, M., & Armaghani, D. J. (2021f). A combination of fuzzy Delphi method and ANN-based models to investigate factors of flyrock induced by mine blasting. Natural Resources Research, 30(2), 1905-1924.

Li, E., Yang, F., Ren, M., Zhang, X., Zhou, J., & Khandelwal, M. (2021d). Prediction of blasting mean fragment size using support vector regression combined with five optimization algorithms. Journal of Rock Mechanics and Geotechnical Engineering, 13(6), 1380-1397.

Li, E., Zhou, J., Shi, X., Jahed Armaghani, D., Yu, Z., Chen, X., & Huang, P. (2021e). Developing a hybrid model of salp swarm algorithm-based support vector machine to predict the strength of fiber-reinforced cemented paste backfill. Engineering with Computers, 37(4), 3519-3540.

Li, J., Li, C., & Zhang, S. (2022d). Application of Six Metaheuristic Optimization Algorithms and Random Forest in the uniaxial compressive strength of rock prediction. Applied Soft Computing, 131, 109729.

Little TN (2007) Flyrock risk. In: Proceedings EXPLO, pp 3–4.

Little, T. N., & Blair, D. P. (2010). Mechanistic Monte Carlo models for analysis of flyrock risk. Rock Fragmentation by Blasting, 9, 641–647.

Liu, B., Wang, R., Zhao, G., Guo, X., Wang, Y., Li, J., & Wang, S. (2020). Prediction of rock mass parameters in the TBM tunnel based on BP neural network integrated simulated annealing algorithm. Tunnelling and Underground Space Technology, 95, 103103.

Lu, X., Hasanipanah, M., Brindhadevi, K., Bakhshandeh Amnieh, H., & Khalafi, S. (2020). ORELM: a novel machine learning approach for prediction of flyrock in mine blasting. Natural Resources Research, 29(2), 641-654.

Lundberg, S. M., & Lee, S. I. (2017). A unified approach to interpreting model predictions. Advances in neural information processing systems, 30.

Lundborg N, Persson A, Ladegaard-Pedersen A, Holmberg R (1975). Keeping the lid on flyrock in open-pit blasting. Eng Min J 176:95–100.

Luo, J., Chen, H., Hu, Z., Huang, H., Wang, P., Wang, X., ... & Wen, C. (2019). A new kernel extreme learning machine framework for somatization disorder diagnosis. Ieee Access, 7, 45512-45525.

Mahdiyar, A., Hasanipanah, M., Armaghani, D. J., Gordan, B., Abdullah, A., Arab, H., & Majid, M. Z. A. (2017). A Monte Carlo technique in safety assessment of slope under seismic condition. Engineering with Computers, 33(4), 807-817.

Majdi, A., & Beiki, M. (2010). Evolving neural network using a genetic algorithm for predicting the deformation modulus of rock masses. International Journal of Rock Mechanics and Mining Sciences, 47(2), 246-253.

Marto, A., Hajihassani, M., Jahed Armaghani, D., Tonnizam Mohamad, E., & Makhtar, A. M. (2014). A novel approach for blast-induced flyrock prediction based on imperialist competitive algorithm and artificial neural network. The Scientific World Journal. https://doi.org/10.1155/2014/643715.

McKenzie, C. K. (2009, February). Flyrock range and fragment size prediction. In Proceedings of the 35th annual conference on explosives and blasting technique (Vol. 2). International Society of Explosives Engineers.

Mikaeil, R., Bakhtavar, E., Hosseini, S., & Jafarpour, A. (2022). Fuzzy classification of rock engineering indices using rock texture characteristics. Bulletin of Engineering Geology and the Environment, 81(8), 312.

Moayedi, H., & Armaghani, J. D. (2018). Optimizing an ANN model with ICA for estimating bearing capacity of driven pile in cohesionless soil. Engineering with Computers, 34(2), 347-356.

Moayedi, H., Gör, M., Lyu, Z., & Bui, D. T. (2020). Herding Behaviors of grasshopper and Harris hawk for hybridizing the neural network in predicting the soil compression coefficient. Measurement, 152, 107389.

Momeni, E., Yarivand, A., Dowlatshahi, M. B., & Armaghani, D. J. (2021). An efficient optimal neural network based on gravitational search algorithm in predicting the deformation of geogrid-reinforced soil structures. Transportation geotechnics, 26, 100446.

Monjezi, M., Amini Khoshalan, H., & Yazdian Varjani, A. (2012). Prediction of flyrock and backbreak in open pit blasting operation: a neuro-genetic approach. Arabian Journal of Geosciences, 5(3), 441-448.

Monjezi, M., Bahrami, A., & Varjani, A. Y. (2010). Simultaneous prediction of fragmentation and flyrock in blasting operation using artificial neural networks. International Journal of Rock Mechanics and Mining Sciences, 3(47), 476-480.

Monjezi, M., Bahrami, A., Varjani, A. Y., & Sayadi, A. R. (2011). Prediction and controlling of flyrock in blasting operation using artificial neural network. Arabian Journal of Geosciences, 4(3), 421-425.

Monjezi, M., Hasanipanah, M., & Khandelwal, M. (2013). Evaluation and prediction of blast-induced ground vibration at Shur River Dam, Iran, by artificial neural network. Neural Computing and Applications, 22(7), 1637-1643.

Murlidhar, B. R., Kumar, D., Jahed Armaghani, D., Mohamad, E. T., Roy, B., & Pham, B. T. (2020). A novel intelligent ELM-BBO technique for predicting distance of mine blasting-induced flyrock. Natural Resources Research, 29(6), 4103-4120.

Murlidhar, B. R., Nguyen, H., Rostami, J., Bui, X., Armaghani, D. J., Ragam, P., & Mohamad, E. T. (2021). Prediction of flyrock distance induced by mine blasting using a novel Harris Hawks optimization-based multi-layer perceptron neural network. Journal of Rock Mechanics and Geotechnical Engineering, 13(6), 1413-1427.

Nguyen, H., Bui, X. N., Choi, Y., Lee, C. W., & Armaghani, D. J. (2021). A novel combination of whale optimization algorithm and support vector machine with different kernel functions for prediction of blasting-induced fly-rock in quarry mines. Natural Resources Research, 30(1), 191-207.

Nguyen, H., Bui, X. N., Nguyen-Thoi, T., Ragam, P., & Moayedi, H. (2019). Toward a state-of-the-art of fly-rock prediction technology in open-pit mines using EANNs model. Applied Sciences, 9(21), 4554.

Nikafshan Rad, H., Bakhshayeshi, I., Wan Jusoh, W. A., Tahir, M. M., & Foong, L. K. (2020). Prediction of flyrock in mine blasting: a new computational intelligence approach. Natural Resources Research, 29(2), 609-623.

Olofsson, S.O., 1990. Applied Explosives Technology for Construction and Mining. Applex Publisher, Arla, Sweden.

Rad, H. N., Hasanipanah, M., Rezaei, M., & Eghlim, A. L. (2018). Developing a least squares support vector machine for estimating the blast-induced flyrock. Engineering with Computers, 34(4), 709-717.

Raina, A. K., Murthy, V. M. S. R., & Soni, A. K. (2014). Flyrock in bench blasting: a comprehensive review. Bulletin of Engineering Geology and the Environment, 73(4), 1199-1209.

Rezaei, M., Monjezi, M., & Varjani, A. Y. (2011). Development of a fuzzy model to predict flyrock in surface mining. Safety science, 49(2), 298-305.

Richards, A., Moore, A., 2004. Flyrock controle By chance or design. In: The Proceedings of the 30th Annual Conference on Explosives and Blasting Technique. The International Society of Explosives Engineers, New Orleans, Louisiana, USA, pp. 335e348.

Roth, J. (1979). A model for the determination of flyrock range as a function of shot conditions. NTIS.

Saghatforoush, A., Monjezi, M., Shirani Faradonbeh, R., & Jahed Armaghani, D. (2016). Combination of neural network and ant colony optimization algorithms for prediction and optimization of flyrock and back-break induced by blasting. Engineering with Computers, 32(2), 255-266.

Shariati, M., Mafipour, M. S., Ghahremani, B., Azarhomayun, F., Ahmadi, M., Trung, N. T., & Shariati, A. (2020). A novel hybrid extreme learning machine–grey wolf optimizer (ELM-GWO) model to predict compressive strength of concrete with partial replacements for cement. Engineering with Computers, 1-23.

Singh, T. N., & Singh, V. (2005). An intelligent approach to prediction and control ground vibration in mines. Geotechnical & Geological Engineering, 23(3), 249-262.

Trivedi, R., Singh, T. N., & Gupta, N. (2015). Prediction of blast-induced flyrock in opencast mines using ANN and ANFIS. Geotechnical and Geological Engineering, 33(4), 875-891.

Trivedi, R., Singh, T. N., & Raina, A. K. (2014). Prediction of blast-induced flyrock in Indian limestone mines using neural networks. Journal of Rock Mechanics and Geotechnical Engineering, 6(5), 447-454.

Trivedi, R., Singh, T. N., & Raina, A. K. (2016). Simultaneous prediction of blast-induced flyrock and fragmentation in opencast limestone mines using back propagation neural network. International Journal of Mining and Mineral Engineering, 7(3), 237-252.

Vapnik, V. N. (1995). The nature of statistical learning. Theory.

Wang, M., Chen, H., Li, H., Cai, Z., Zhao, X., Tong, C., ... & Xu, X. (2017). Grey wolf optimization evolving kernel extreme learning machine: Application to bankruptcy prediction. Engineering Applications of Artificial Intelligence, 63, 54-68.

Wang, M., Shi, X., & Zhou, J. (2018a). Charge design scheme optimization for ring blasting based on the developed Scaled Heelan model. International Journal of Rock Mechanics and Mining Sciences, 110, 199-209.

Wang, M., Shi, X., Zhou, J., & Qiu, X. (2018b). Multi-planar detection optimization algorithm for the interval charging structure of large-diameter longhole blasting design based on rock fragmentation aspects. Engineering Optimization, 50(12), 2177-2191.

Wang, S., Jia, H., Abualigah, L., Liu, Q., & Zheng, R. (2021). An improved hybrid aquila optimizer and harris hawks algorithm for solving industrial engineering optimization problems. Processes, 9(9), 1551.

Wang, X., Hosseini, S., Jahed Armaghani, D., & Tonnizam Mohamad, E. (2023). Data-Driven Optimized Artificial Neural Network Technique for Prediction of Flyrock Induced by Boulder Blasting. Mathematics, 11(10), 2358.

Wang, X., Tang, Z., Tamura, H., Ishii, M., & Sun, W. D. (2004). An improved backpropagation algorithm to avoid the local minima problem. Neurocomputing, 56, 455-460.

Yagiz, S., Ghasemi, E., & Adoko, A. C. (2018). Prediction of rock brittleness using genetic algorithm and particle swarm optimization techniques. Geotechnical and Geological Engineering, 36(6), 3767-3777.

Yang, Z., Duan, H., Fan, Y., & Deng, Y. (2018). Automatic carrier landing system multilayer parameter design based on Cauchy mutation pigeon-inspired optimization. Aerospace Science and Technology, 79, 518-530.

Yari, M., Bagherpour, R., Jamali, S., & Shamsi, R. (2016). Development of a novel flyrock distance prediction model using BPNN for providing blasting operation safety. Neural Computing and Applications, 27(3), 699-706.

Ye, J., Koopialipoor, M., Zhou, J., Armaghani, D. J., & He, X. (2021). A novel combination of tree-based modeling and Monte Carlo simulation for assessing risk levels of flyrock induced by mine blasting. Natural Resources Research, 30(1), 225-243.

Zhang, H., Nguyen, H., Bui, X. N., Pradhan, B., Asteris, P. G., Costache, R., & Aryal, J. (2021). A generalized artificial intelligence model for estimating the friction angle of clays in evaluating slope stability using a deep neural network and Harris Hawks optimization algorithm. Engineering with Computers, 1-14.

Zhang, H., Wu, S., & Zhang, Z. (2022). Prediction of Uniaxial Compressive Strength of Rock Via Genetic Algorithm—Selective Ensemble Learning. Natural Resources Research, 31(3), 1721-1737.

Zhang, W., & Goh, A. T. (2016). Multivariate adaptive regression splines and neural network models for prediction of pile drivability. Geoscience Frontiers, 7(1), 45-52.

Zhou, J., Aghili, N., Ghaleini, E. N., Bui, D. T., Tahir, M. M., & Koopialipoor, M. (2020a). A Monte Carlo simulation approach for effective assessment of flyrock based on intelligent system of neural network. Engineering with Computers, 36(2), 713-723.

Zhou, J., Bejarbaneh, B.Y., Armaghani, D.J. and Tahir, M.M., (2020b). Forecasting of TBM advance rate in hard rock condition based on artificial neural network and genetic programming techniques. Bulletin of Engineering Geology and the Environment, 79, 2069–2084.

Zhou, J., Dai, Y., Du, K., Khandelwal, M., Li, C., & Qiu, Y. (2022). COSMA-RF: New intelligent model based on chaos optimized slime mould algorithm and random forest for estimating the peak cutting force of conical picks. Transportation Geotechnics, 100806.

Zhou, J., Dai, Y., Khandelwal, M., Monjezi, M., Yu, Z., & Qiu, Y. (2021d). Performance of hybrid SCA-RF and HHO-RF models for predicting backbreak in open-pit mine blasting operations. Natural Resources Research, 30(6), 4753-4771.

Zhou, J., Huang, S., Wang, M., & Qiu, Y. (2021a). Performance evaluation of hybrid GA–SVM and GWO–SVM models to predict earthquake-induced liquefaction potential of soil: a multi-dataset investigation. Engineering with Computers, 1-19.

Zhou, J., Koopialipoor, M., Murlidhar, B. R., Fatemi, S. A., Tahir, M. M., Jahed Armaghani, D., & Li, C. (2020c). Use of intelligent methods to design effective pattern parameters of mine blasting to minimize flyrock distance. Natural Resources Research, 29(2), 625-639.

Zhou, J., Li, E., Yang, S., Wang, M., Shi, X., Yao, S. and Mitri, H.S. (2019). Slope stability prediction for circular mode failure using gradient boosting machine approach based on an updated database of case histories. Safety Science, 118, pp.505-518.

Zhou, J., Qiu, Y., Armaghani, D. J., Zhang, W., Li, C., Zhu, S., & Tarinejad, R. (2021c). Predicting TBM penetration rate in hard rock condition: a comparative study among six XGB-based metaheuristic techniques. Geoscience Frontiers, 12(3), 101091.

Zhou, J., Qiu, Y., Zhu, S., Armaghani, D. J., Li, C., Nguyen, H., & Yagiz, S. (2021b). Optimization of support vector machine through the use of metaheuristic algorithms in forecasting TBM advance rate. Engineering Applications of Artificial Intelligence, 97, 104015.

Zhu, L., Zhang, C., Zhang, C., Zhou, X., Wang, J., & Wang, X. (2018). Application of Multiboost-KELM algorithm to alleviate the collinearity of log curves for evaluating the abundance of organic matter in marine mud shale reservoirs: a case study in Sichuan Basin, China. Acta Geophysica, 66(5), 983-1000.

Zou, T., & Wang, C. (2022). Adaptive Relative Reflection Harris Hawks Optimization for Global Optimization. Mathematics, 10(7), 1145.